J. Phys. G: Nucl. Part. Phys. **24** (1998) 1657–1691. Printed in the UK PII: S0954-3899(98)86234-8

TOPICAL REVIEW

Photon–photon physics in very peripheral collisions of relativistic heavy ions

Gerhard Baur†§, Kai Hencken‡‖ and Dirk Trautmann‡¶

† Institut für Kernphysik, Forschungszentrum Jülich, Postfach 1913, D–52425 Jülich, Germany
‡ Institut für Physik, Universität Basel, Klingelbergstrasse 82, CH–4056 Basel, Switzerland

Received 23 April 1998

Abstract. In central collisions at relativistic heavy ion colliders such as the Relativistic Heavy Ion Collider (RHIC), Brookhaven and the Large Hadron Collider (LHC) (in its heavy ion mode) at CERN, Geneva, one aims at detecting a new form of hadronic matter—the quark gluon plasma. It is the purpose of this review to discuss a complementary aspect of these collisions, the very peripheral ones. Owing to coherence, there are strong electromagnetic fields of short duration in such collisions. They give rise to photon–photon and photon–nucleus collisions with high flux up to an invariant mass region hitherto unexplored experimentally. After a general survey photon–photon luminosities in relativistic heavy ion collisions are discussed. Special care is taken to include the effects of strong interactions and nuclear size. Then photon–photon physics at various $\gamma\gamma$-invariant mass scales is discussed. The region of several GeV, relevant for RHIC is dominated by quantum chronodynamics phenomena (meson and vector meson pair production). Invariant masses of up to about 100 GeV can be reached at LHC, and the potential for new physics is discussed. Photonuclear reactions and other important background effects, especially diffractive processes are also discussed. A special chapter is devoted to lepton-pair production, especially electron–positron pair production; owing to the strong fields new phenomena, especially multiple e^+e^- pair production, will occur there.

1. Introduction

The parton picture is very useful to study scattering processes at very high energies. In this model the scattering is described as an incoherent superposition of the scattering of the various constituents. For example, nuclei consist of nucleons which in turn consist of quarks and gluons, photons consist of lepton pairs, electrons consist of photons, etc. It is the subject of this topical review to discuss that relativistic nuclei have photons as an important constituent, especially for low enough virtuality $Q^2 = -q^2 > 0$ of the photon. This is due to the coherent action of all the charges in the nucleus. The virtuality of the photon is related to the size R of the nucleus by

$$Q^2 \lesssim 1/R^2 \tag{1}$$

the condition for coherence. The radius of a nucleus is given approximately by $R = 1.2\ \mathrm{fm}\ A^{1/3}$, where A is the nucleon number. From the kinematics of the process one has

$$Q^2 = \frac{\omega^2}{\gamma^2} + Q_\perp^2.$$

§ E-mail address: G.Baur@fz-juelich.de
‖ E-mail address: hencken@quasar.physik.unibas.ch
¶ E-mail address: trautmann@ubaclu.unibas.ch

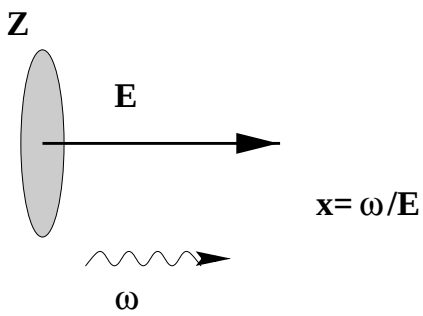

Figure 1. A fast-moving nucleus with charge Ze is surrounded by a strong electromagnetic field. This can be viewed as a cloud of virtual photons. These photons can often be considered as real. They are called equivalent or quasireal photons. The ratio of the photon energy ω and the incident beam energy E is denoted by $x = \omega/E$. Its maximal value is restricted by the coherence condition to $x < \lambda_C(A)/R \approx 0.175/A^{4/3}$, that is, $x \lesssim 10^{-3}$ for Ca ions and $x \lesssim 10^{-4}$ for Pb ions.

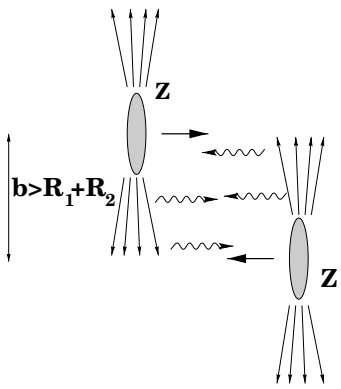

Figure 2. Two fast-moving electrically charged objects are an abundant source of (quasireal) photons. They can collide with each other and with the other nucleus. For peripheral collisions with impact parameters $b > 2R$, this is useful for photon–photon as well as photon–nucleus collisions.

Owing to the coherence condition, the maximum energy of the quasireal photon is therefore given by

$$\omega_{\max} \approx \frac{\gamma}{R} \tag{2}$$

and the maximum value of the perpendicular component is given by

$$Q_\perp \lesssim \frac{1}{R}.$$

We define the ratio $x = \omega/E$, where E denotes the energy of the nucleus $E = M_N \gamma A$ and M_N is the nucleon mass. It is therefore smaller than

$$x_{\max} = \frac{1}{R M_N A} = \frac{\lambda_C(A)}{R} \tag{3}$$

here $\lambda_C(A)$ is the Compton wavelength of the ion. Hereafter we use natural units, setting $\hbar = c = 1$.

The collisions of e^+ and e^- has been the traditional way to study $\gamma\gamma$-collisions. Similarly photon–photon collisions can also be observed in hadron–hadron collisions. Since the photon number scales with Z^2 (Z being the charge number of the nucleus) such effects can be particularly large. Of course, the strong interaction of the two nuclei has to be taken into consideration.

The equivalent photon flux present in medium- and high-energy nuclear collisions is very high, and has found many useful applications in nuclear physics [1], nuclear astrophysics [2, 3], particle physics [4] (sometimes called the 'Primakoff effect'), as well as, atomic physics [5]. It is the main purpose of this review to discuss the physics of photon–photon and photon–hadron (nucleus) collisions in high-energy heavy ion collisions. With

the construction of the 'Relativistic Heavy Ion Collider' (RHIC) and the 'Large Hadron Collider' (LHC) scheduled for 1999 and for 2004/2008, respectively, one will be able to investigate such collisions experimentally. The main purpose of these heavy ion colliders is the formation and detection of the quark–gluon plasma, a new form of highly excited dense hadronic matter. Such a state of matter will be created in central collisions. The present interest is in the 'very peripheral (distant) collisions', where the nuclei do not interact strongly with each other. From this point of view, grazing collisions and central collisions are considered as a background. It is needless to say that this 'background' can also be interesting physics of its own.

The equivalent photon spectrum extends up to several GeV at RHIC energies ($\gamma \approx 100$) and up to about 100 GeV at LHC energies ($\gamma \approx 3000$), see equation (2). Therefore the range of invariant masses $M_{\gamma\gamma}$ at RHIC will be up to about the mass of the η_c, at LHC it will extend into an invariant mass range hitherto unexplored.

We discuss the equivalent photon spectra of strongly interacting particles, from which $\gamma\gamma$-luminosities are obtained. Owing to the coherence effect, the corresponding $\gamma\gamma$-luminosity is very high. In addition higher order and inelastic processes, which may occur in heavy ion collisions are discussed. Then the various possibilities for $\gamma\gamma$-physics in the different invariant mass regions will be explored. A special case of $\gamma\gamma$-physics is lepton pair production, in particular the e^+e^- pair production. Since the equivalent photon approximation fails in some regions of phase space, this case is discussed separately. Owing to its strong-field aspects, the production of multiple e^+e^- pairs is of basic interest. Electron–positron pair creation is also of practical interest due to the possibility of capturing a electron in a K, L, ... shell. This changes the charge state of the ion and leads to a beam loss and thus to a decrease in the luminosity. The very large cross section for the production of e^+e^- pairs (sometimes called quantum electrodynamic (QED) electrons) is also an important background for detectors.

Relativistic heavy ion collisions were suggested as a general tool for two-photon physics about a decade ago. Yet the study of a special case, the production of e^+e^- pairs in nucleus–nucleus collisions, goes back to the work of Landau and Lifschitz in 1934 [6]. (In those days, of course, one thought more about high-energy cosmic-ray nuclei than relativistic heavy ion colliders). In the meantime the importance of this process has become very clear, and many studies followed, e.g. [7–9]. This subject will be dealt with in detail in sections 5 and 7, where also recent experimental results will be mentioned.

The general possibilities and characteristic features of two-photon physics in relativistic heavy ion collisions have been discussed in [9]. The possibility to produce a Higgs boson via $\gamma\gamma$-fusion was suggested in [10, 11]. In these papers the effect of strong absorption in heavy ion collisions was not taken into account. This absorption is a feature, which is quite different from the two-photon physics at e^+e^- colliders. The problem of taking strong interactions into account was solved by using impact parameter space methods in [12–14]. Thus the calculation of $\gamma\gamma$-luminosities in heavy ion collisions is put on a firm basis and rather definite conclusions were reached by many groups working in the field [15]; for a recent review containing further references see [16]. Subsequent studies—to be described in detail in this review—revealed in a clear way that the theoretical situation is basically understood. This opens the way for many interesting applications. Until now hadron–hadron collisions have not been used for two-photon physics. An exception can be found in [17]. There the production of $\mu^+\mu^-$ pairs at the ISR was observed. The special class of events was selected, where no hadrons are seen associated with the muon pair in a large solid angle vertex detector. In this way one makes sure that the hadrons do not interact strongly with each other, i.e. one is dealing with peripheral collisions (with impact

parameters $b > 2R$); the photon–photon collisions manifest themselves as 'silent events'.

We feel that this is a very good basis for planning concrete experiments, as is done at RHIC [17–20] and LHC [21–23]. This review aims at giving the main physical ideas and providing the key formula and results. Details can be found in the literature. A few new results will also be presented, but the main emphasis is to discuss the principle ideas and results in the field. We hope that this review will further stimulate future investigations. It is appropriate to recall that RHIC will start operating in 1999, only a year from now.

2. General survey of peripheral collisions

Let us first discuss the importance of electromagnetic interactions in peripheral collisions for the case of elastic scattering. The strength of the Coulomb interaction is measured by the Coulomb (or Sommerfeld) parameter η which is given in terms of the nuclear charges Z_1 and Z_2 by

$$\eta = \frac{Z_1 Z_2 e^2}{\hbar v}. \tag{4}$$

For (ultra)relativistic collisions we have $v \approx c$ and thus $\eta \approx Z_1 Z_2/137$. Therefore for proton–proton (pp) collisions we have always $\eta \ll 1$ and the Born approximation, that is, one-photon exchange, is applicable. For this case, i.e. for $\eta \approx \frac{1}{137}$, elastic scattering is reviewed, e.g. in [25]. (Experimental results for $p\bar{p}$ scattering at $\sqrt{s} = 546$ and 1800 GeV at Fermilab are given in [25–27].) There is a superposition of nuclear and Coulomb amplitudes and the elastic differential scattering cross section is divided into three distinct regions, separated by the value of the square of the momentum transfer t. It is defined as usual as $t = (p_i - p_f)^2$, which is negative (spacelike momentum transfer) in the metric we use. For $|t| \ll |t|_{\rm int}$ Coulomb scattering dominates, for $|t| \gg |t|_{\rm int}$, nuclear scattering dominates and for $|t| \approx |t|_{\rm int}$ there is Coulomb-nuclear interference. $|t|_{\rm int}$ is given by (see equation (3.13) of [25], where the factor of $Z_1 Z_2$ is added for the scattering of two nuclei with charge Z_1,Z_2 instead of two protons)

$$|t|_{\rm int} \approx \frac{8\pi\alpha Z_1 Z_2}{\sigma_{\rm tot}}. \tag{5}$$

The nuclear elastic scattering amplitude is usually parametrized as

$$F_n = \frac{(\rho + i)\sigma_{\rm tot}}{4\sqrt{\pi}} {\rm e}^{Bt/2} \tag{6}$$

where $\sigma_{\rm tot}$ is the total cross section, $\rho = \frac{{\rm Re}\, f_{\rm c.m.}(0)}{{\rm Im}\, f_{\rm c.m.}(0)}$ and B is a slope parameter related to the size of the hadron. In this normalization the differential cross section is given by

$$\frac{{\rm d}\sigma}{{\rm d}t} = |F_n|^2. \tag{7}$$

On the other hand for (very) heavy ions we have $\eta \gg 1$ and semiclassical methods are appropriate to deal with elastic scattering (see also [29]). For $\eta \gg 1$ the Coulomb interaction is very strong and the Born approximation is no longer valid. (In analogy with optics there is now Fraunhofer diffraction instead of Fresnel diffraction.) Instead, one should use a Glauber approximation, where the Coulomb interaction is taken into account to all orders. One can say that many photons are typically exchanged in the elastic collisions (in contrast to the Born approximation relevant for the pp case, where one photon exchange is sufficient). One can now integrate over the impact parameter b using the saddle-point approximation. Thus one recovers the classical picture of scattering. The particles move

essentially on a straight line with a constant velocity and an impact parameter b. For $Z_1 = Z_2 = Z$ at grazing impact parameter $b = 2R$ the momentum transfer is given by (see, e.g. [30])

$$|t|_{\mathrm{Coul}} = (\Delta p)^2 = \left(\frac{2Z^2e^2}{2Rv}\right)^2 \approx \frac{Z^4e^4}{R^2c^2}. \tag{8}$$

This momentum transfer determines the scattering angle $\theta = \Delta p/p$, where p is the momentum of the particle.

Let us compare this quantity with the corresponding one for pp-scattering, equation (5). With $\sigma_{\mathrm{tot}} \approx 8\pi R^2$ one has

$$|t|_{\mathrm{int}} = \frac{\alpha Z^2}{R^2} \tag{9}$$

to be compared with

$$|t|_{\mathrm{Coul}} = \frac{\alpha Z^2}{R^2}(\alpha Z^2). \tag{10}$$

It seems interesting to note that $|t|_{\mathrm{Coul}}$ is $Z^2\alpha$ times the corresponding quantity $|t|_{\mathrm{int}}$. Evidently the corresponding scattering angles are exceedingly small. For $\eta \approx 1$, i.e. for $Z \approx 12$, the quantities $|t|_{\mathrm{int}}$ and $|t|_{\mathrm{Coul}}$ (equations (9) and (10)) are about equal, as should be the case. For such values of Z the change from Fresnel to Fraunhofer scattering takes place. A more detailed discussion is given in chapter 5.3.4 of [31], based on the work of [32].

The pp cross section is rising with energy (see, e.g. p 193 of [33]). At LHC energies it will be of the order of 80 mbarn. What does this mean for the p–A and A–A cross sections? A discussion is given in [34]. Experimental information can be obtained from cosmic-ray data for p–A reactions. Calculations of the cross section for A–A data often make use of a density-folding approach. This approach can be justified starting from Glauber theory [35, 36]. One uses the thickness function $T_A(b)$ of each nucleus, which is defined as the projection of the density along the beam axis:

$$T_A(b) = \int_{-\infty}^{+\infty} \mathrm{d}z n_A(\sqrt{b^2 + z^2}). \tag{11}$$

Here the nuclear density $n_A(r)$ is normalized to $\int \mathrm{d}^3r\ n_A(r) = A$. From this one obtains the 'overlap function' given by

$$T_{AB}(b) = \int \mathrm{d}^2b_1 \int \mathrm{d}^2b_2\, t(\boldsymbol{b} - \boldsymbol{b}_1 - \boldsymbol{b}_2) T_A(b_1) T_B(b_2) \tag{12}$$

where $\boldsymbol{b}$ is the impact parameter between the two ions (see also figure 3).

$t(\boldsymbol{s})$ describes the finite range of the nucleon–nucleon (NN) interaction. It is proportional to the profile function $\Gamma(b)$ in the Glauber theory, but it is normalized to $\int \mathrm{d}^2s\, t(\boldsymbol{s}) = 1$. Therefore we have $\int \mathrm{d}^2b\, T_{AB}(b) = AB$. For high energies the NN cross section rises beyond the geometrical size of the protons. The finite range of the NN interaction is important then. A similar situation also occurs in nuclear physics at lower energies, see, e.g. figures 2 and 3 of [37], where the influence of the finite range of the NN interaction is clearly seen on the total cross section for scattering of Li and Be isotopes.

If the nucleon–nucleon cross section is almost purely absorptive, the scattering amplitude is almost imaginary and one can get $t(b)$ from the elastic differential cross section

$$t(\boldsymbol{s}) = \frac{\int \mathrm{d}^2p_\perp\ \exp(\mathrm{i}\boldsymbol{p}_\perp\boldsymbol{s})\sqrt{\frac{\mathrm{d}\sigma}{\mathrm{d}^2p_\perp}}}{(2\pi)^2\ \sqrt{\frac{\mathrm{d}\sigma}{\mathrm{d}^2p_\perp}}\Big|_{p_\perp=0}} \tag{13}$$

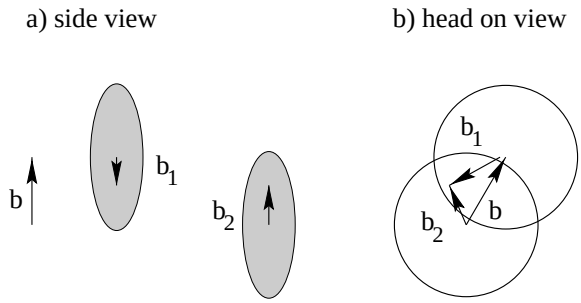

Figure 3. The probability of the nucleus to interact in central collisions can be described within the ρ–ρ folding approach to the Glauber theory. The parameters b, b_1 and b_2 used in the text are explained.

with $\frac{d\sigma}{d^2 p_\perp}$ the elastic nucleon–nucleon cross section. Often $t(\boldsymbol{b})$ is approximated by an exponential function of the form $t(\boldsymbol{b}) \sim \exp(-(b/b_0)^2)$, where b_0 is the range of the interaction.

If one can neglect the finite range of the interaction compared with the geometrical size of the nuclei, the 'thickness function' can be simplified:

$$T_{AB}(b) = \int d^2 b_1 \int d^2 b_2\, \delta^{(2)}(b - b_1 - b_2) T_A(b_1) T_B(b_2) \tag{14}$$

$$= \int d^2 b_1\, T_A(b_1) T_B(b - b_1). \tag{15}$$

The inelastic scattering cross section of the nucleus–nucleus collision is given by

$$\sigma_{AB,\mathrm{inel}} = \int d^2 b\, [1 - \exp(-\sigma_{\mathrm{NN}} T_{AB}(b))] \tag{16}$$

where σ_{NN} is the total nucleon–nucleon cross section. This integration over b allows the integrand to be interpreted as a probability for the two ions to interact. This probability is about 1 for small impact parameters, where the nuclei overlap, it drops to zero for large impact parameters. The width of the area, where it falls off, is given by the surface diffuseness of the nuclear densities and the range of the nucleon–nucleon interaction as given by t. Similarly the elastic cross section is given by

$$\sigma_{AB,\mathrm{el}} = \int d^2 b\, [1 - \exp(-\sigma_{\mathrm{NN}} T_{AB}(b)/2)]^2. \tag{17}$$

Using results from Regge theory (see, e.g. [38, 39]) one can estimate the range b_0 of the interaction by

$$b_0 = 2\sqrt{B_{0,pP} + \ln(s/s_0)\alpha'_P}. \tag{18}$$

Using for $B_{0,pP} \approx 2.4\ \mathrm{GeV}^{-2}$ and for $\alpha'_P \approx 0.25\ \mathrm{GeV}^{-2}$, as found in [38, 39], one gets for LHC energies ($s = (2 \times 7\ \mathrm{TeV})^2$, $s_0 = 1\ \mathrm{GeV}^2$) $b_0 \approx 1$ fm, which is small compared with the nuclear radius.

As we will see in the next section, the photon–photon luminosity depends also on the probability for the two nuclei to interact with each other. Only those processes, where the ions do not interact, are useful for photon–photon physics. From our discussion here, we can conclude that the effect of the increasing range of the NN interaction will only be of some importance at the very high end of the invariant $\gamma\gamma$-masses for a quantitative determination of the photon–photon luminosity.

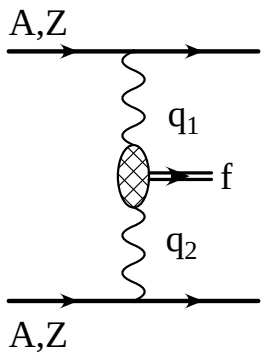

Figure 4. The general Feynman diagram of photon–photon processes in heavy ion collisions. Two (virtual) photons fuse in a charged particle collision into a final system f.

3. From impact-parameter dependent equivalent photon spectra to $\gamma\gamma$-luminosities

Photon–photon collisions have been studied extensively at e^+e^- colliders. The theoretical framework is reviewed, e.g. in [40]. The basic graph for the two-photon process in ion-ion collisions is shown in figure 4. Two virtual (spacelike) photons collide to form a final state f. In the equivalent photon approximation it is assumed that the square of the four-momentum of the virtual photons is small, i.e. $q_1^2 \approx q_2^2 \approx 0$ and the photons can be treated as quasireal. In this case the $\gamma\gamma$-production is factorized into an elementary cross section for the process $\gamma + \gamma \to f$ (with real photons, i.e. $q^2 = 0$) and a $\gamma\gamma$-luminosity function. In contrast to the pointlike elementary electrons (positrons), nuclei are extended, strongly interacting objects with internal structure. This gives rise to modifications in the theoretical treatment of two-photon processes.

3.1. Elastic vertices

The emission of a photon depends on the (elastic) form factor. Often a Gaussian form factor or one of a homogeneous charged sphere is used. The typical behaviour of a form factor is

$$f(q^2) \approx \begin{cases} Z & \text{for } |q^2| < \frac{1}{R^2} \\ 0 & \text{for } |q^2| \gg \frac{1}{R^2}. \end{cases} \tag{19}$$

For low $|q^2|$ all the protons inside the nucleus act coherently, whereas for $|q^2| \gg 1/R^2$ the form factor is very small, close to 0. For a medium size nucleus with, say, $R = 5$ fm, the limiting $Q^2 = -q^2 = 1/R^2$ is given by $Q^2 = (40\ \text{MeV})^2 = 1.6 \times 10^{-3}\ \text{GeV}^2$. Apart from e^+e^- (and to a certain extent also $\mu^+\mu^-$) pair production—which will be discussed separately below—this scale is much smaller than typical scales in the two-photon processes. Therefore the virtual photons in relativistic heavy ion collisions can be treated as quasireal. This is a limitation as compared with e^+e^- collisions, where the two-photon processes can also be studied as a function of the corresponding masses q_1^2 and q_2^2 of the exchanged photon ('tagged mode').

As already discussed in the previous section, relativistic heavy ions interact strongly when the impact parameter is smaller than the sum of the radii of the two nuclei. In such cases $\gamma\gamma$-processes are still present and are a background that has to be considered in central collisions. In order to study 'clean' photon–photon events however, they have to be eliminated in the calculation of photon–photon luminosities as the particle production owing to the strong interaction dominates. In the usual treatment of photon–photon processes in e^+e^- collisions plane waves are used and there is no direct information on the impact

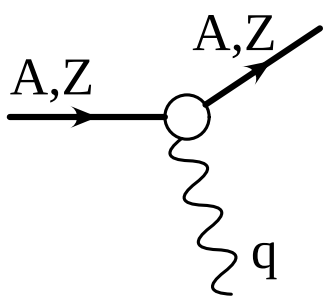

Figure 5. 'Elastic photon emission'. In order for the photon to interact coherently with the whole nucleus, its virtuality Q^2 is restricted to $Q^2 \lesssim 1/R^2$. In the calculation this is incorporated by the elastic form factor $f(q^2)$. This is important for a treatment, where plane waves are used. In the semiclassical (or Glauber) method, the detailed form of $f(q^2)$ is not relevant for collisions with $b > R$ (see text).

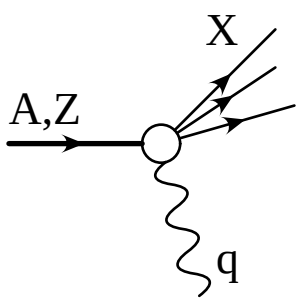

Figure 6. 'Inelastic photon emission'. As a nucleus is a rather weakly bound system, photon emission can lead to its break-up or excitation, especially for $Q^2 \gtrsim 1/R^2$. Also for this incoherent case an equivalent photon number, similar to the coherent case, can be defined.

parameter. For heavy ion collisions on the other hand it is very appropriate to introduce impact-parameter dependent equivalent photon numbers. They have been widely discussed in the literature (see e.g. [1, 30, 41]).

The equivalent photon spectrum corresponding to a point charge Ze, moving with a velocity v at impact parameter b is given by

$$N(\omega, b) = \frac{Z^2\alpha}{\pi^2}\frac{1}{b^2}\left(\frac{c}{v}\right)^2 x^2\left[K_1^2(x) + \frac{1}{\gamma^2}K_0^2(x)\right] \tag{20}$$

where $K_n(x)$ are the modified Bessel functions (MacDonald functions) [42] and $x = \frac{\omega b}{\gamma v}$. Then one obtains the probability for a certain electromagnetic process to occur in terms of the same process generated by an equivalent pulse of light as

$$P(b) = \int \frac{\mathrm{d}\omega}{\omega} N(\omega, b)\sigma_\gamma(\omega). \tag{21}$$

Possible modifications of $N(\omega, b)$ owing to an extended spherically symmetric charge distribution are given in [43] (see also equation (47) below). It should be noted that equation (20) also describes the equivalent photon spectrum of an extended charge distribution, such as a nucleus, as long as b is larger than the extension of the object. This is due to the fact that the electric field of a spherically symmetric system depends only on the total charge, which is inside it. As one often wants to avoid final state interaction between the produced system and the nuclei, one has to restrict oneself to $b_i > R_i$ and therefore the form factor is not very important. For inelastic vertices a photon number $N(\omega, b)$ can also be defined, as will be discussed in section 3.2 below.

As the term $x^2[K_1^2(x) + 1/\gamma^2 K_0^2(x)]$ in equation (20) can be roughly approximated as 1 for $x < 1$ and 0 for $x > 1$, so that the equivalent photon number $N(\omega, b)$ is almost a constant up to a maximum $\omega_{\max} = \gamma/b$ ($x = 1$). By integrating the photon spectrum (equation (20)) over b from a minimum value of $R_{\min}$ up to infinity (where essentially only impact parameters up to $b_{\max} \approx \gamma/\omega$ contribute, cf equation (2)), one can define an

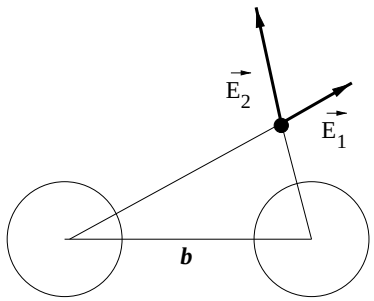

Figure 7. View of the collision perpendicular to the beam direction. The electric field vector points along the direction of the individual impact parameter.

equivalent photon number $n(\omega)$. This integral can be carried out analytically and is given by [1, 30]

$$n(\omega) = \int \mathrm{d}^2 b\, N(\omega, b) = \frac{2}{\pi} Z_1^2 \alpha \left(\frac{c}{v}\right)^2 \left[\xi K_0 K_1 - \frac{v^2 \xi^2}{2c^2}(K_1^2 - K_0^2)\right] \tag{22}$$

where the argument of the modified Bessel functions is $\xi = \frac{\omega R_{\min}}{\gamma v}$. The cross section for a certain electromagnetic process is then

$$\sigma = \int \frac{\mathrm{d}\omega}{\omega} n(\omega) \sigma_\gamma(\omega). \tag{23}$$

Using the approximation above for the MacDonald functions, we get an approximated form, which is quite reasonable and is useful for estimates:

$$n(\omega) \approx \frac{2Z^2\alpha}{\pi} \ln \frac{\gamma}{\omega R_{\min}}. \tag{24}$$

The photon–photon production cross section is obtained in a similar factorized form, by folding the corresponding equivalent photon spectra of the two colliding heavy ions [13, 14] (for polarization effects see [13], they are neglected here)

$$\sigma_c = \int \frac{\mathrm{d}\omega_1}{\omega_1} \int \frac{\mathrm{d}\omega_2}{\omega_2} F(\omega_1, \omega_2) \sigma_{\gamma\gamma}(W_{\gamma\gamma} = \sqrt{4\omega_1\omega_2}) \tag{25}$$

with

$$F(\omega_1, \omega_2) = 2\pi \int_{R_1}^{\infty} b_1\, \mathrm{d}b_1 \int_{R_2}^{\infty} b_2\, \mathrm{d}b_2 \int_0^{2\pi} \mathrm{d}\phi \times N(\omega_1, b_1) N(\omega_2, b_2) \Theta(b_1^2 + b_2^2 - 2b_1 b_2 \cos\phi - R_{\text{cut-off}}^2) \tag{26}$$

($R_{\text{cut-off}} = R_1 + R_2$). This can also be rewritten in terms of the invariant mass $W_{\gamma\gamma} = \sqrt{4\omega_1\omega_2}$ and the rapidity $Y = \frac{1}{2}\ln((P_0 + P_z)/(P_0 - P_z)) = \frac{1}{2}\ln(\omega_1/\omega_2)$ as

$$\sigma_c = \int \mathrm{d}W_{\gamma\gamma}\, \mathrm{d}Y \frac{\mathrm{d}^2 L}{\mathrm{d}W_{\gamma\gamma}\, \mathrm{d}Y} \sigma_{\gamma\gamma}(W_{\gamma\gamma}) \tag{27}$$

with

$$\frac{\mathrm{d}^2 L_{\gamma\gamma}}{\mathrm{d}W_{\gamma\gamma} \mathrm{d}Y} = \frac{2}{W_{\gamma\gamma}} F\left(\frac{W_{\gamma\gamma}}{2}\mathrm{e}^{Y}, \frac{W_{\gamma\gamma}}{2}\mathrm{e}^{-Y}\right). \tag{28}$$

Here energy and momentum in the beam direction are denoted by P_0 and P_z. The transverse momentum is of the order of $P_\perp \leqslant 1/R$ and is neglected here. The transverse momentum distribution is calculated in [44].

In [44, 45] this intuitively plausible formula is derived *ab initio*, starting from the assumption that the two ions move on a straight line with impact parameter b. Equations (25)

and (27) are the basic formulae for $\gamma\gamma$-physics in relativistic heavy ion collisions. The advantage of heavy nuclei is seen in the coherence factor $Z_1^2 Z_2^2$ contained in equations (25)–(28).

Let us make a few remarks. In equation (26) a sharp cut-off in impact parameter space at $b_{\min} = R_{\text{cut-off}}$ is introduced. There is some ambiguity in the numerical value of $R_{\text{cut-off}}$: As was discussed in section 2 the total cross section for nucleon–nucleon collisions is rising with energy. To a certain extent this will also affect the values of $R_{\text{cut-off}}$. They are not just the (energy-independent) radii of the nuclei, but they rather describe the probability of nuclear interactions between the heavy ions. A more realistic calculation can be done by replacing this sharp cut-off with a smooth one, using the overlap function of equation (15) and (12). The Θ-function in equation (26) has to be replaced by

$$P(b) = 1 - \exp(-\sigma_{\text{NN}} T_{AB}(b)) \tag{29}$$

with $\boldsymbol{b} = \boldsymbol{b}_1 - \boldsymbol{b}_2$. Comparing this refined model with the one with a sharp cut-off, significant deviations are only present at the very upper end of the invariant mass range. Only the smallest impact parameters contribute significantly to these events, therefore a sensitivity to the cut-off is expected. All other (smaller) invariant masses are not very sensitive to the details of this cut-off.

Integrating over all Y the cross section is

$$\sigma_c = \int \mathrm{d}W_{\gamma\gamma} \frac{\mathrm{d}L}{\mathrm{d}W_{\gamma\gamma}} \sigma_{\gamma\gamma}(W_{\gamma\gamma}). \tag{30}$$

For symmetric collisions ($R_1 = R_2 = R$) we can write the luminosity in terms of a universal function $f(\tau)$ as

$$\frac{\mathrm{d}L}{\mathrm{d}W_{\gamma\gamma}} = \frac{Z^4\alpha^2}{\pi^4} \frac{1}{W_{\gamma\gamma}} f(\tau) \tag{31}$$

with $\tau = W_{\gamma\gamma} R/\gamma$ [14]. For large values of γ, $f(\tau)$ is given by

$$f(\tau) = \pi\tau^2 \int_1^\infty u_1\,\mathrm{d}u_1 \int_1^\infty u_2\,\mathrm{d}u_2 \int_0^{2\pi} \mathrm{d}\phi\,\Theta(u_1^2 + u_2^2 - 2u_1u_2\cos\phi - 4) \int_{-\infty}^{+\infty} \mathrm{d}Y\, K_1^2\left(\frac{\tau}{2}u_1 \mathrm{e}^{Y}\right) K_1^2\left(\frac{\tau}{2}u_2 \mathrm{e}^{-Y}\right). \tag{32}$$

The function $f(\tau)$ is shown in figure 8, a useful parametrization of it was studied in [14].

As a function of Y, the luminosity $\mathrm{d}^2L/\mathrm{d}W_{\gamma\gamma}\mathrm{d}Y$ has a Gaussian shape with the maximum at $Y = 0$. The width is approximately given by $\Delta Y = 2\ln[(2\gamma)/(RW_{\gamma\gamma})]$. Depending on the experimental situation additional cuts in the allowed Y range are needed.

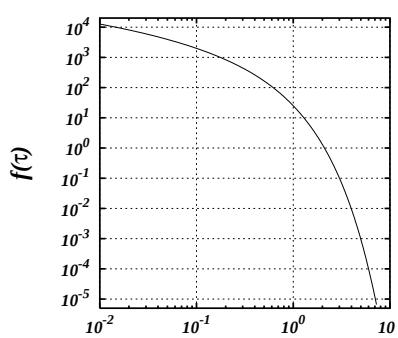

Figure 8. Plot of the universal function $f(\tau)$ (see equation (32)) as a function of $\tau = W_{\gamma\gamma} R/\gamma$.

Table 1. Parameters for different ion species at RHIC and LHC. In the entries we give the total invariant mass $\sqrt{s}$ of the system, the Lorentz factor γ and the beam luminosity. Parameters are taken from [23, 21].

Ion	Z, A	$\sqrt{s}$	γ	L_{AA} (cm^{-2} s^{-1})
LHC				
Pb–Pb	82,208	1148 TeV	2950	1×10^{26}
Ca–Ca	20,40	280 TeV	3750	4×10^{30}
p–p	1,1	14 TeV	7450	10^{29}–10^{31}
RHIC				
Au–Au	79,197	20 TeV	106	2×10^{26}
I–I	53,127	13 TeV	111	3×10^{27}
Cu–Cu	29,63	7.2 TeV	122	1×10^{28}
Si–Si	14,28	3.5 TeV	133	4×10^{28}
O–O	8,16	2.0 TeV	133	1×10^{29}
p–p	1,1	250 GeV	266	1×10^{31}

3.2. Inelastic vertices and higher order corrections

Heavy ions are complex objects unlike the pointlike, structureless electrons. The effects owing to the finite size (and the nuclear interactions between them) has been considered by using an impact parameter approach. The additional processes coming from elastic nuclear interactions (diffractive processes, Pomeron interactions) will be considered separately in sections 4 and 6. Here we wish to discuss mainly additional electromagnetic processes that can occur in distant collisions.

Especially for very heavy ions, such as Pb, $Z\alpha$ is no longer small. Therefore processes with more than one photon-exchange are important. In addition to the $\gamma\gamma$-process one can have electromagnetic dissociation of the ions. Furthermore the ions can also be excited owing to the emission of the photon. This excitation can lead to an excited nucleus, or to the break-up of the nucleus, when the proton is knocked out of the nucleus owing to the photon emission. At even higher Q^2 the photon can also be emitted from the quarks contained in the protons.

In section 4 we will see that the electromagnetic dissociation of the ions is an important process. This cross section is often so large that it can also occur in addition to the $\gamma\gamma$-process.

In the impact-parameter dependent approach the probability of several processes to occur in one collision can be calculated by assuming that the processes are independent of each other; their probabilities have to multiplied:

$$P_{fA^*}(b) = P_{\gamma\gamma\to f}(b)\ P_{\gamma A\to A^*}(b). \tag{33}$$

Therefore the processes given in figure 9 are effectively included in this approach. This is a good approximation as long as the nucleus is not disturbed substantially. Integrating from $b = 2R$ up to infinity, one obtains the cross section for $\gamma\gamma \to f$ fusion accompanied by a specific $\gamma A \to A^*$ interaction

$$\sigma_{fA^*} = 2\pi \int_{2R}^{\infty} b\,\mathrm{d}b\, P_{\gamma\gamma\to f}(b) P_{\gamma A\to A^*}(b). \tag{34}$$

Since $\sum_{A^*} P_{\gamma A\to A^*} = 1$ (where we sum over all possible states A^* of the nucleus including the ground state), we have

$$\sum_{A^*} \sigma_{fA^*} = \sigma_f \tag{35}$$

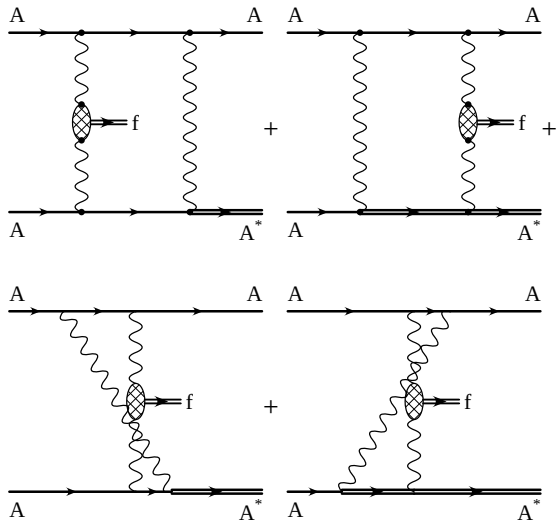

Figure 9. Owing to the large charge of the ions, electromagnetic excitation in addition to the photon–photon process may occur.

that is, the same as the cross section of the $\gamma\gamma \to f$ process alone, without any higher order processes, as given above.

One can make an estimate of the importance of the higher order processes in the following way. The luminosity, especially at high invariant masses peaks at $b \approx b_{\min} = 2R$ and one can therefore make the approximation

$$\sigma_{f,A} \approx P_A(2R)\sigma_{\gamma\gamma\to f} \tag{36}$$

for the cross section $\sigma_{f,A}$, that is $\gamma\gamma \to f$ with the nucleus in the ground state in the final state and

$$\sigma_{f,A^*} \approx (1 - P_a(2R))\sigma_{\gamma\gamma\to f} \tag{37}$$

for the nucleus to be excited. The impact-parameter dependent probability for the excitation of the nucleus can be found in [1, 45–47]. They are strongly dependent on A. Particularly important (see also section 4) is the giant dipole resonance (GDR), a highly coherent excited state, which can be interpreted as the movement of all neutrons against all protons. The probability of such an excitation of a nucleus with charge Z_2 and nucleon number A_2 ($N_2 = A_2 - Z_2$) by a nucleus with charge number Z_1 is given in [1] as

$$P_{\mathrm{GDR}}(b) = 1 - \exp(-S/b^2) \tag{38}$$

with

$$S = 5.45 \times 10^{-5} \frac{Z_2^2 N_2 Z_2}{A_2^{2/3}} \ \mathrm{fm}^2 \tag{39}$$

where the Thomas–Reiche–Kuhn (TRK) sum rule was used and the position of the GDR is given by $80A^{-1/3}$ MeV. For Pb–Pb we get a value of $S = (10.4\ \mathrm{fm})^2$. A parametrization which also includes all additional contributions (quasideuteron absorption, nucleon excitation, etc) was given in [49]; they get a value of $S = (17.4\ \mathrm{fm})^2$. For the system Ca–Ca we get $S = (0.86\ \mathrm{fm})^2$ using equation (39).

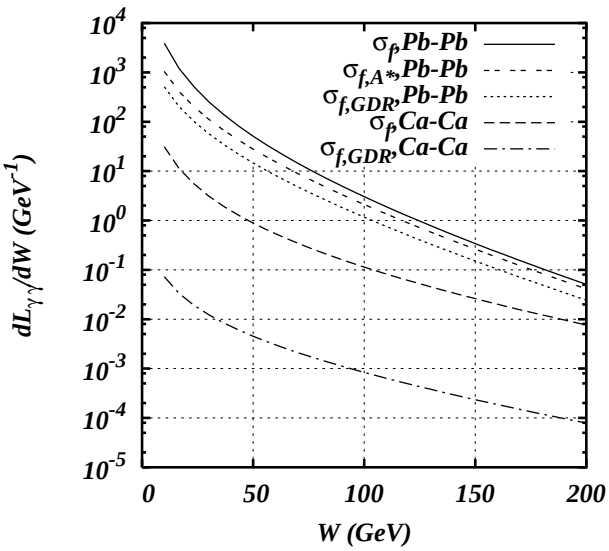

Figure 10. For Pb–Pb collisions a substantial portion of the total luminosity (σ_f, full curve) comes from events with are accompanied by the excitation of at least one ion (σ_{A*}, double-dashed curve) The dominant contribution is to the giant dipole resonance (σ_{GDR}, dotted curve). For Ca–Ca collisions this is no longer very important. Shown are full calculations for the LHC ($\gamma \approx 2950$ for Pb–Pb, 3750 for Ca–Ca).

From this estimate one finds that about 75% of the photon–photon events in Pb–Pb collisions are accompanied by an excitation, about 40% leading to the GDR. For Ca–Ca these are less than 2% of all events. As each of the ions can be excited, we get a total probability for excitation of at least one of them of about 2% for Ca–Ca and of about 95% for Pb–Pb (65% from GDR). These effects are therefore dominant for Pb–Pb, but almost insignificant for Ca–Ca.

A detailed calculation of the cross section using the full b dependence is shown in figure 10. It shows that the excitation probability is lower than the estimate given above.

The GDR excitation is followed most of the time by neutron evaporation. Also other photon-induced reactions predominantly lead to the emission of individual nucleons. This emission of relatively low-energy nucleons in the nucleus rest frame leads to highly-energetic neutrons (protons) with energies of about 3 TeV (LHC) or 100 GeV (RHIC). The neutrons can possibly be detected in a zero-degree calorimeter.

In [50] it was proposed to use the mutual emission of neutrons from both nuclei as a measure of the beam luminosity at RHIC. Using the coincidence of two neutrons in the very forward and backward direction other sources of neutrons can be suppressed effectively. Since the photonuclear processes are large and well understood they can lead to a good determination of the luminosity. The authors of [50] estimate to be able to determine the luminosity to about 5%. It seems interesting to note that the A dependence of the excitation cross section with two photons is given approximately by $10^{-9}A^6$ mb [12], the one-photon exchange cross section is given approximately by $10^{-5}A^2$ mb [51], see figure 11. So for nuclei heavier than about C, the two-photon mechanism is dominant over the one-photon mechanism.

In the calculation of the luminosity we were always assuming that both nuclei remain in their ground state; but nuclei are weakly bound composite systems and it is possible

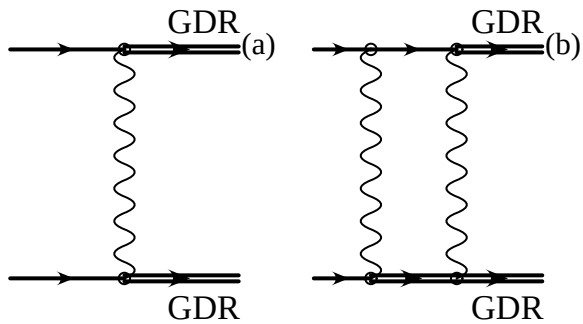

Figure 11. The mutual excitation process (*a*), where both ions are excited owing to one-photon exchange, becomes less important at larger A compared with (*b*) the second-order process.

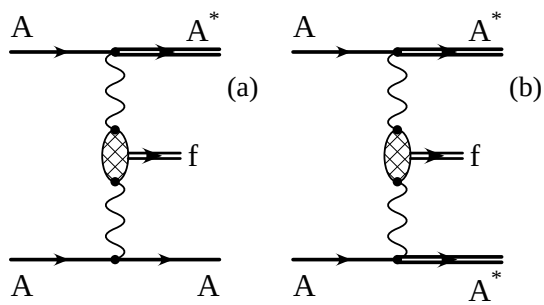

Figure 12. In photon–photon collisions, (*a*) one and (*b*) even both nuclear vertices can be inelastic, leading to excited nuclei.

that the photon emission leads to their excitation (see also figure 12). We distinguish two different types: those leading to an excited nucleus with a well defined excitation and the incoherent photon emission from individual protons (or even quarks within the protons), which are best treated as inclusive processes, summing over all excitation energies.

An equation for the inelastic photon-emission to a discrete state, was derived in [52] (see also [40]) using plane waves and therefore not subtracting the central collisions. It was applied to nuclear excitation, as well as to the case of the proton-delta transition [53]. The equivalent photon number can be expressed in terms of the structure functions C and D of the general hadron tensor

$$\overline{\sum_{M_i M_f}} \Gamma^{\mu *}\Gamma^{\nu} = \left[g^{\mu\nu} - \frac{q^{\mu}q^{\nu}}{q^2}\right] C + \left[P^{\mu} - \frac{qP}{q^2}q^{\mu}\right]\left[P^{\nu} - \frac{qP}{q^2}q^{\nu}\right] D \qquad (40)$$

where Γ_{μ} denotes the nuclear four-current. One obtains

$$n(\omega) = \int \frac{(-2C + q_{\perp}/\omega^2 \;\; P^2 D)\omega^2}{(2\pi)^3 2EP(q^2)^2}\, \mathrm{d}^2 q_i \qquad (41)$$

where E and P are energy and momentum of the nucleus. Whereas in the elastic case q^2 was given by $-(\omega^2/\gamma^2 + q_{\perp}^2)$, it is here $\approx -\left[\frac{\omega}{\gamma}\left(\frac{\omega}{\gamma} + 2\Delta\right)\right]$, where Δ is the excitation energy. Using the Goldhaber–Teller model, the transition to the GDR was found to be very small, below 1% of the elastic contribution. Using the elastic structure functions of the proton in its usual dipole form (see, e.g. [40]) the elastic proton equivalent photon

number was obtained analytically in [54]. Quite similarly the equivalent photon number corresponding to the p–Δ transition was obtained analytically in [53] using the structure functions of [55] as

$$n_{\mathrm{p}\to\Delta}(\omega) = \frac{\alpha}{4\pi}\frac{\mu^{*2}}{9m^2}\left(\frac{m^*+m}{2m}\right)^2\left[t_{\min}\left\{\ln\left(\frac{t_{\min}}{\Lambda^2+t_{\min}}\right)+\frac{11}{6}-\frac{2t_{\min}}{\Lambda^2+t_{\min}}\right.\right.$$
$$\left.\left.+\frac{3t_{\min}^2}{2(\Lambda^2+t_{\min})^2}-\frac{t_{\min}^3}{3(\Lambda^2+t_{\min})^3}\right\}+\frac{\Lambda^8}{3(\Lambda^2+t_{\min})^3}\right] \tag{42}$$

with

$$t_{\min} = \frac{\omega^2}{\gamma^2}+\frac{(m^*-m)^2}{\gamma^2}+2\frac{\omega(m^*-m)}{\gamma} \tag{43}$$

and where $m^* = 1232$ MeV is the mass of the Δ, $m = 938$ MeV the proton mass, $\Lambda^2 = 0.71$ GeV^2 and $\mu^* = 9.42$. For not too large photon energy ω it is given by a constant

$$n_\Delta(\omega) \approx \frac{\alpha}{4\pi}\frac{\mu^{*2}}{9m^2}\left(\frac{m^*+m}{2m}\right)^4\frac{\Lambda^2}{3}. \tag{44}$$

This is an effect of the order of 10% [53].

As we have seen above, the knowledge of impact-parameter dependent equivalent photon numbers is very helpful, as it allows in a direct way to take the strong absorption into account (equation (26)). The equivalent photon spectrum corresponding to a fast-moving point particle is given by equation (20). This result can now be generalized to arbitrary charge-current distributions (also quantum mechanical transition currents in the framework of the Glauber theory).

The equivalent photon spectrum corresponding to a spherically symmetric charge distribution $\rho(r)$ moving with velocity v at an impact parameter b is derived in [43]. The Fourier transformation of this charge distribution, with $\int \mathrm{d}^3r\rho(r) = Z$, is given by

$$f(k^2) = ZF(k^2) = \int \mathrm{d}^3r\,\exp(-\mathrm{i}\boldsymbol{k}\boldsymbol{r})\rho(r). \tag{45}$$

For $\gamma \gg 1$ we only need the perpendicular component of the electric and magnetic fields, $\boldsymbol{E}_\perp$ and $\boldsymbol{B}_\perp$. One finds [43]

$$\boldsymbol{E}_\perp = \int \frac{\mathrm{d}^2k_\perp}{(2\pi)^2}\frac{Ze}{vk^2}f(k^2)\exp(-\mathrm{i}\boldsymbol{k}_\perp\boldsymbol{b})\boldsymbol{k}_\perp \tag{46}$$

where $k^2 \approx -k_\perp^2-(\omega/\gamma)^2$. It can easily be seen, that $E_\perp \parallel \boldsymbol{b}$ and one obtains the equivalent photon number as

$$N(\omega,b) = \frac{Z^2\alpha}{\pi^2}\left(\frac{c}{v}\right)^2\frac{1}{b^2}\left|\int_0^\infty \mathrm{d}u\,u^2J_1(u)\frac{f(-\frac{x^2+u^2}{b^2})}{x^2+u^2}\right|^2 \tag{47}$$

where $x = \omega b/\gamma$.

In a similar way the equivalent photon spectrum of a pointlike magnetic dipole, moving with a constant velocity at a given impact parameter, is calculated in [56]. This purely classical result can also be interpreted quantum mechanically by using the corresponding electromagnetic matrix elements.

An interesting question is the incoherent contributions due to the protons inside the nucleus. We generalize equations (45)–(47) in the following way. The static charge

distribution is replaced by a transition charge density $\rho_{f0}(r)$ and the Fourier transform of it is given by

$$f_{f0}(\boldsymbol{k}) = \int \mathrm{d}^3 r \, \exp(-\mathrm{i}\boldsymbol{k}\boldsymbol{r})\rho_{f0}(r) \tag{48}$$

where f is some final state of the nucleus and

$$f_{f0}(\boldsymbol{k}) = \int \mathrm{d}^3 r \, \mathrm{d}\xi \, \Psi_f^*(\xi) \sum_{i=1}^{Z} \delta(\boldsymbol{r} - \boldsymbol{r}_i)\Psi_0(\xi) \exp(-\mathrm{i}\boldsymbol{k}\boldsymbol{r}) \tag{49}$$

$$= \sum_{i=1}^{Z} \int \mathrm{d}\xi \, \Psi_f^*(\xi) \exp(-\mathrm{i}\boldsymbol{k}\boldsymbol{r}_i)\Psi_0(\xi) \tag{50}$$

where $\xi = r_1, r_2, \ldots, r_Z$ is the set of all proton coordinates (for our argument we can neglect the neutrons). We get the total incoherent contribution by summing over all states f excluding the ground state $f = 0$. The sum can be performed using the closure relation and we obtain:

$$\begin{aligned} S(\boldsymbol{k}, \boldsymbol{k}') = \sum_{f \neq 0} f_{f0}^*(\boldsymbol{k}) f_{f0}(\boldsymbol{k}') &= \int \mathrm{d}\xi \, \mathrm{d}\xi' \sum_{i,j} \Psi_0^*(\xi) \exp(\mathrm{i}\boldsymbol{k}\boldsymbol{r}_i)\Psi_f(\xi)\Psi_f^*(\xi') \\ &\quad \times \exp(-\mathrm{i}\boldsymbol{k}'\boldsymbol{r}_j')\Psi_0(\xi') - f_{00}^*(\boldsymbol{k}) f_{00}(\boldsymbol{k}') \\ &= \sum_{i,j} \int \mathrm{d}\xi \, |\Psi_0(\xi)|^2 \exp(\mathrm{i}\boldsymbol{k}\boldsymbol{r}_i - \mathrm{i}\boldsymbol{k}'\boldsymbol{r}_j) - f_{00}^*(\boldsymbol{k}) f_{00}(\boldsymbol{k}'). \end{aligned} \tag{51}$$

We split the sum over i, j now into one for $i = j$ and one for $i \neq j$, following [57]. In the limit of no correlation (not even Pauli correlations) we obtain

$$S(\boldsymbol{k}, \boldsymbol{k}') = ZF(\boldsymbol{k} - \boldsymbol{k}') - ZF(\boldsymbol{k})F(\boldsymbol{k}') \tag{52}$$

where we have introduced a normalized form factor $F(\boldsymbol{k})$ of the nucleus as $F(\boldsymbol{k}) = f_{00}(\boldsymbol{k})/Z$, i.e. $F(0) = 1$.

The equivalent photon number owing to the incoherent contribution can now be written as

$$N^{\mathrm{incoh}}(\omega, b) = \frac{\alpha}{\pi^2} \left(\frac{c}{v}\right)^2 \frac{1}{b^2} \int\!\!\int \mathrm{d}^2 k_\perp \, \mathrm{d}^2 k_\perp' \boldsymbol{k}_\perp \boldsymbol{k}_\perp' \frac{\exp(\mathrm{i}\boldsymbol{k}_\perp \boldsymbol{b} - \mathrm{i}\boldsymbol{k}_\perp' \boldsymbol{b})}{k^2 k'^2} S(\boldsymbol{k}, \boldsymbol{k}') \tag{53}$$

where $\boldsymbol{k} = (\boldsymbol{k}_\perp, \omega/v)$, $\boldsymbol{k}' = (\boldsymbol{k}_\perp', \omega/v)$. Using equations (45) and (52) and defining a thickness function $T_z(b)$, see equation (11), where the nucleon density n_A is now replaced by the charge density ρ, we have

$$N^{\mathrm{incoh}}(\omega, b) = \int \mathrm{d}^2 r_\perp \, T_z(r_\perp) N^{\mathrm{point}}(\omega, \boldsymbol{b} + \boldsymbol{r}_\perp) - ZN^{\mathrm{form}}(\omega, b) \tag{54}$$

where N^{form} is the usual equivalent photon number for a given form factor (divided by Z^2), see equation (47), N^{point} denotes the equivalent photon spectrum owing to a point charge. For $b = 0$ this expression would diverge, and a suitable cut-off has to be introduced ($b_{\mathrm{min}} = R_{\mathrm{proton}}$, or another value of b_{min}, for which the equivalent photon approximation ceases to be valid). If one is integrating over all impact parameters (therefore also including central collisions), the total incoherent equivalent photon number can be defined:

$$n^{\mathrm{incoh}}(\omega) = Z[n^{\mathrm{point}}(\omega) - n^{\mathrm{form}}(\omega)] \tag{55}$$

where $n^i(\omega) = \int \mathrm{d}^2 b \, N^i(\omega, b)$ and we have used $\int \mathrm{d}^2 r_\perp \, T_z(\boldsymbol{r}_\perp) = Z$.

Incoherent scattering is a well known general phenomenon. For example, the blue sky is caused by the incoherent scattering of sunlight by gas molecules or other randomly

distributed dipole scatterer (see, e.g. p 418 of [30]). It can also be formulated in a way that makes a connection with the parton model. As an example let us look at the contribution from incoherent photon emissions of the quarks in the proton. In the parton model a proton in the infinite-momentum frame consists of partons (quarks, gluons, ...). We use the plane-wave approach (see [40]), where the impact-parameter dependence is not manifest. The equivalent photon spectrum corresponding to a given proton final state can be expressed in terms of the structure functions W_1 and W_2. We only consider the dominant term corresponding to W_2. We are also interested only in inclusive reactions, therefore we integrate over the invariant mass of the final state M^2. One has [40, 58]

$$n(\omega) = \frac{\alpha}{\pi} \iint \frac{\mathrm{d}Q^2\,\mathrm{d}M^2}{(Q^2)^2} |q_\perp|^2 \frac{1}{2m} W_2(M^2, Q^2) \tag{56}$$

with $Q^2 = Q^2_{\min}(\omega) + q_\perp^2$. Since $p = p' + q$ we obtain

$$M^2 = m^2 + 2m\nu - Q^2 \tag{57}$$

with $\nu = -pq/m$. (Since we assume that the photon is emitted, not absorbed, from the nuclear system, our sign of q and ν is somewhat unconventional.) Introducing the scaling variable $x = Q^2/(2m\nu)$, we can write in the scaling limit, see e.g. [58],

$$W_2(M^2, Q^2) = \frac{1}{\nu} F_2(x). \tag{58}$$

Changing the integration variable $\mathrm{d}M^2$ to $\mathrm{d}x$, we obtain

$$n(\omega) = \frac{\alpha}{\pi} \int \mathrm{d}x\, F_2(x) \frac{1}{x} \int \mathrm{d}Q^2\, \frac{|q_\perp|^2}{(Q^2)^2}. \tag{59}$$

We express the structure function $F_2(x)$ in terms of the quark distribution functions $f_{q_i|p}(x)$:

$$F_2(x) = x \sum_{q_i} e_i^2 f_{q_i|p}(x) \tag{60}$$

where e_i is the charge of the quark q_i ($i = u, d, s, \ldots$). Equation (59) now has an intuitive interpretation: The proton consist of partons (=quarks) with a momentum fraction x, they radiate as pointlike particles. This is described by the $\mathrm{d}Q^2$ integration. Taking also the energy loss of the quarks into account in a more complete formula, the photon spectrum from a quark is given by

$$f_{\gamma/q}(z) = \frac{\alpha}{2\pi} \frac{1 + (1-z)^2}{z} \log\left(\frac{Q_1^2}{Q_2^2}\right) \tag{61}$$

where z is the ratio of photon-energy ω and energy of the quark xE.

According to [59] we choose Q_1^2 to be the maximum value of the momentum transfer given by $x_1x_2z_1z_2s/4 - m^2$ and the choice of the minimum $Q_2^2 = 1\ \mathrm{GeV}^2$ is made such that the photons are sufficiently off-shell for the quark–parton model to be applicable. The inelastic contribution to the $\gamma\gamma$-cross section is then given by

$$\begin{aligned}\sigma_{\mathrm{pp}}^{\mathrm{inel}} = \sum_{ij} e_i^2 e_j^2 \int_{\frac{4m^2}{s}}^1 \mathrm{d}x_1 \int_{\frac{4m^2}{sx_1}}^1 \mathrm{d}x_2 \int_{\frac{4m^2}{sx_1x_2}}^1 \mathrm{d}z_1 \int_{\frac{4m^2}{sx_1x_2z_1}}^1 \mathrm{d}z_2 \\ f_{q_i|p}(x_1, Q^2) f_{q_j|p}(x_2, Q^2) f_{\gamma/q_i}(z_1) f_{\gamma/q_j}(z_2) \\ \hat{\sigma}_{\gamma\gamma}(W_{\gamma\gamma} = \sqrt{x_1x_2z_1z_2s/4})\end{aligned} \tag{62}$$

(equation (3) of [59]) and where s is the invariant mass of the pp system. Of course the photons are now somewhat more off-shell than in the elastic case, and for some cases it

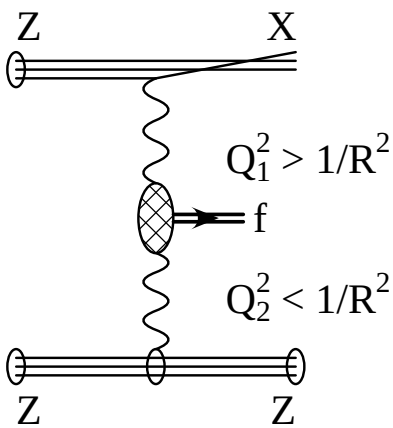

Figure 13. With $Q^2 < 1/R^2$ the photon is emitted coherently from all 'partons' inside the ion. For $Q^2 \gg 1/R^2$ the 'partonic' structure of the ion is resolved.

could be less safe to use the assumption of real photons ($q^2 = 0$), when calculating the cross section for the $\gamma\gamma$-subprocess $\hat{\sigma}$.

A similar formula can also be written for the semi-elastic (=elastic–inelastic) cross section, see [59, 60]. $\gamma\gamma$-luminosities are calculated according to this procedure in both of these papers. The MRSD parametrization [61, 62] for the partonic densities is used in [59], in [60] the simple parametrization $F_2 = 0.16\ln(1/x)$ was used. One finds that typically the inel–inel contribution is largest, as the charges of the partons (quarks) are comparable to the charges of the proton.

For the proton contribution to the photon spectrum of a heavy nucleus, the situation is different. The coherent contribution is proportional to Z^2, whereas they are only proportional to Z for the incoherent one. As $Z \gg 1$ one expects the coherent part to be dominant.

4. γ–A interactions

The cross section for the collisions of the equivalent photons of one nucleus with the other is given by (see equation (23)):

$$\sigma = \int \frac{\mathrm{d}\omega}{\omega} n(\omega)\sigma_\gamma(\omega). \tag{63}$$

where the equivalent photon number $n(\omega)$ is given in equation (22) and $\sigma_\gamma(\omega)$ is the photonuclear cross section. This gives rise to many interesting phenomena ranging from the excitation of discrete nuclear states, giant multipole resonances (especially the GDR), quasideuteron absorption, nucleon resonance excitation to the nucleon continuum (see, e.g. [33, 63]). Photoinduced processes lead in general to a change of the charge-to-mass ratio of the nuclei, and with their large cross section they are therefore a serious source of beam loss. In particular, the cross section for the excitation of the the GDR, a collective mode of the nucleus, is rather large for the heavy systems (of the order of 100 barn). For a recent discussion see [64]. The cross section scales approximately with $Z^{10/3}$. (Another serious source of beam loss, the e^+e^- bound–free pair creation will be discussed in section 7.) The contribution of the nucleon resonances (especially the Δ resonance) has also been confirmed experimentally in fixed-target experiments with 60 and 200 GeV/A (heavy ions at CERN, 'electromagnetic spallation') [63–65]. For details of these aspects, we refer the reader to [16, 47, 48, 69], where scaling laws, as well as detailed calculations for individual cases are given.

Recently the total dissociation cross section for different ion species was studied in an experiment at CERN [70]. There it was found that this cross section is dominated at medium and large Z by the electromagnetic dissociation, with the region of the GDR contributing with about 80%. The theoretical calculations, which can be considered to be fairly reliable and detailed, see e.g. [71], agree quite well with the experiments apart from an additional effect, which can be parametrized as $\sigma_{\mathrm{add}} = 0.12Z$ barn, a very sizeable effect (for large Z it is even larger than the nuclear cross section). It is tempting to guess that the Z dependence is due to an incoherent effect of the Z protons in a nucleus. However, the corresponding incoherent photon number (equation (54)) is very small for the relevant region $b > R_1 + R_2$. Therefore we exclude an incoherent effect as the explanation of the anomaly observed in [70].

The interaction of quasireal photons with protons has been studied extensively at the electron–proton collider HERA (DESY, Hamburg), with $\sqrt{s} = 300$ GeV ($E_{\mathrm{e}} = 27.5$ GeV and $E_{\mathrm{p}} = 820$ GeV in the laboratory system). This is made possible by the large flux of quasireal photons from the electron (positron) beam (for a review see [38]). The obtained γp centre-of-mass energies (up to $W_{\gamma\mathrm{p}} \approx 200$ GeV) are an order of magnitude larger than those reached by fixed-target experiments. Similar and more detailed studies will be possible at the relativistic heavy ion colliders RHIC and LHC, owing to the larger flux of quasireal photons from one of the colliding nuclei. In the photon–nucleon subsystem, one can reach invariant masses $W_{\gamma\mathrm{N}}$ up to $W_{\gamma\mathrm{N,max}} = \sqrt{4W_{\mathrm{max}}E_{\mathrm{N}}} \approx 0.8\gamma A^{-1/6}$ GeV. In the case of RHIC (^{197}Au, $\gamma = 106$) this is about 30 GeV, for LHC (^{208}Pb, $\gamma = 2950$) one obtains 950 GeV. Thus one can study physics quite similar to that at HERA, with nuclei instead of protons. Photon–nucleon physics includes many aspects, such as the energy dependence of total cross sections, diffractive and non-diffractive processes (see, e.g. [38]). An important subject is elastic vector meson production $\gamma\mathrm{p} \to \mathrm{Vp}$ (with $V = \rho, \omega, \phi, J/\Psi, \ldots$). A review of exclusive neutral vector meson production is given in [72]. The diffractive production of vector mesons allows one to obtain insight into the interface between perturbative QCD and hadronic physics. Elastic processes (i.e. the proton remains in the ground state) have to be described within non-perturbative (and therefore phenomenological) models. It was shown in [73] that diffractive ('elastic') J/Ψ photoproduction is a probe of the gluon density at $x \approx \frac{M_\Psi^2}{W_{\gamma\mathrm{N}}^2}$ (for quasireal photons). Inelastic J/Ψ photoproduction was also studied recently at HERA [74]. Going to the hard exclusive photoproduction of heavy mesons on the other hand, perturbative QCD is applicable. Recent data from HERA on the photoproduction of J/Ψ mesons have shown a rapid increase of the total cross section with $W_{\gamma\mathrm{N}}$, as predicted by perturbative QCD. Such studies could be extended to photon–nucleus interactions at RHIC, thus complementing the HERA studies. Equivalent photon flux factors are large for the heavy ions owing to coherence. On the other hand, the A–A luminosities are quite low, as compared with HERA. Of special interest is the coupling of the photon of one nucleus to the Pomeron-field of the other nucleus. Such studies are envisaged for RHIC, see [17–20] where experimental feasibility studies were also performed.

It is useful to have estimates of the order of magnitude of vector meson production in photon–nucleon processes at RHIC and LHC. Let us assume a cross section that rises with the γp centre-of-mass energy approximately with a power law:

$$\sigma_\gamma = \sigma_0 \left(\frac{W_{\gamma\mathrm{N}}}{W_0} \right)^\beta \tag{64}$$

with W_0 chosen to be 1 GeV and $\beta \approx 0.22$ for $V = \rho, \omega, \phi$, and $\beta \approx 0.8$ for $V = J/\Psi$. Also the total hadronic interaction cross section can be parametrized in this form with $\beta \approx 0.16$. From figure 17 of [38] or figure 5 of [75] one has for $\sigma_0 \approx 50$ μbarn for the

total hadronic cross section, 5 μbarn for $V = \rho$, 0.5 μbarn for $V = \omega$, ϕ and 10^{-3} μbarn for $V = J/\Psi$. Making use of the photon number of equation (24) the total cross section for vector meson production on the reaction $Z + \mathrm{p} \to Z + \mathrm{p} + V$ owing to the equivalent photon spectrum of the nucleus Z is obtained as

$$\sigma = \frac{2Z^2\alpha}{\pi}\sigma_0\left(\frac{2m_\mathrm{N}\gamma_\mathrm{p}}{RW_0^2}\right)^{\beta/2}\left[\left(1-\left(\frac{\omega_\mathrm{min}R}{\gamma_\mathrm{p}}\right)^{\beta/2}\right)\frac{4}{\beta^2}+\left(\frac{\omega_\mathrm{min}R}{\gamma_\mathrm{p}}\right)^{\beta/2}\frac{2\ln\left(\omega_\mathrm{min}R/\gamma_\mathrm{p}\right)}{\beta}\right] \tag{65}$$

where some minimum value of the energy of the equivalent photon is used, say $\omega_\mathrm{min} =$ 1 GeV for the total hadronic cross section, $\omega_\mathrm{min} = 2$ GeV for $V = \rho, \omega$ and ϕ and $\omega_\mathrm{min} = 10$ GeV for $V = J/\Psi$, and $\omega_\mathrm{max} = \gamma_\mathrm{p}/R$. For $\beta = 0$ one obtains in a similar way

$$\sigma = \frac{Z^2\alpha}{\pi}\sigma_0\left[\ln\left(\frac{\gamma_\mathrm{p}}{\omega_\mathrm{min}R}\right)\right]^2. \tag{66}$$

The Lorentz factor γ_p of the nucleus Z, as viewed from the proton, is given by

$$\gamma_\mathrm{p} = 2\gamma^2 - 1. \tag{67}$$

We assume that a proton and a nucleus Z collide, with the same value γ (see figure 1, where one nucleus is replaced by a proton). We obtain the following numbers, shown in table 2.

The numbers in table 2 refer to the photoproduction on one proton. In AA collisions there is incoherent photoproduction on the individual A nucleons. Shadowing effects will occur in the nuclear environment and it will be interesting to study these. There is also the coherent contribution where the nucleus remains in the ground state. Owing to the large momentum transfer, the total (angle integrated) coherent scattering shows an undramatic $A^{4/3}$ dependence. This is in contrast to, e.g. low-energy νA elastic scattering, where the coherence effect leads to an A^2 dependence, which is relevant for stellar collapse, see, e.g. [76], where also a pedagogical general discussion of coherence effects is given. In addition there are inelastic contributions, where the proton (nucleon) is transformed into some final state X during the interaction (see [74]). The experimental possibilities of this at RHIC are investigated in [18, 20, 21].

At the LHC one can extend these processes to much higher invariant masses W, therefore much smaller values of x will be probed. Whereas the J/Ψ production at HERA was measured up to invariant masses of $W \approx 160$ GeV, the energies at the LHC allow for studies up to ≈ 1 TeV.

Table 2. The expected cross sections for the elastic vector meson production on a proton induced by the equivalent photons of a nucleus Z are given for RHIC and LHC conditions. Also shown are the total electromagnetic cross sections σ_tot. See text for details.

	RHIC		LHC	
Ion	I	Au	Ca	Pb
γ	111	106	3750	2950
R (fm)	6	7	4	7
σ_tot (mbarn)	20	40	15	200
σ_ρ (mbarn)	2	3.5	1.5	25
σ_ω, σ_ϕ (mbarn)	0.2	0.35	0.15	2.5
$\sigma_{J/\Psi}$ (μbarn)	0.5	1.5	3	40

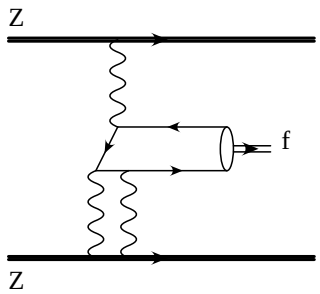

Figure 14. By using three (or more) photon processes also, states that are forbidden in the two-photon fusion process can be produced. Interesting final states f are, for example, orthopositronium, orthomuonium, or the vector mesons ρ, ω, ϕ.

At the FELIX detector at LHC [23] hard diffractive vector meson photoproduction can be investigated especially well in AA collisions. In comparison with previous experiments, the very large photon luminosity should allow observation of processes with quite small γp cross sections, such as Υ-production. For more details see [23].

$C = -1$ vector mesons can be produced in principle by the fusion of three (or, less important, five, seven, ...) equivalent photons (see figure 14). The cross section scales with Z^6. This graph has been calculated by Ginzburg *et al* [77] using the methods of [78–80]. It is smaller than the contributions discussed above, even for nuclei with large Z. Quite similarly the QED analogue of the $C = -1$ mesons, the orthostates of positronium, muonium, or tauonium can be calculated [81].

One may have thought that these three or more photon contributions are of the same order of magnitude, since $Z\alpha \leqslant 1$. However, there is another scale: as one can see from equation (74) below, there is another factor $1/(mb)$. For electrons the important range $b \approx 1/m$ and this factor therefore is of the order of unity. From this one expects that orthopositronium production can be similar in size to parapositronium production. For heavier systems the impact parameter range b cannot be smaller than R, the nuclear radius. Putting $1/R = \Lambda \approx 30$ MeV (for $R \approx 7$ fm), the scale factor is Λ/M with M the mass of the produced particle $M = m_\mu, \ldots$. This factor is always (much) smaller than one, thus the production via these higher order processes is small. Of course the above arguments are rather qualitative and should be complemented by more detailed calculations. Such calculations can be done using the technique developed for vector meson production in proton-proton collisions via gluon-exchange processes [74–76].

As another possibility we mention photon–gluon fusion leading to the production of $c\bar{c}$ and $b\bar{b}$ quark pairs. It was suggested in [82] as a possibility to deduce the in-medium gluon distribution. Further studies were done in [83, 84], and this possibility is reviewed in [16].

5. Photon–photon physics at various invariant mass scales

Scattering of light on light, while absent in classical Maxwell electrodynamics, takes place owing to quantum effects, such as pair creation. At low energies, photon–photon scattering is dominated by electron intermediate states, the scattering of light on light occurs in higher orders via an electron loop, see, e.g. [85]. The lowest order process is e^+e^- pair creation and is well described by QED.

Until now photon–photon scattering has been mainly studied at e^+e^- colliders. Many reviews [83–86] as well as conference reports [88–91] exist. The traditional range of invariant masses has been the region of mesons, ranging from π^0 ($m_{\pi^0} = 135$ MeV) up to about η_c ($m_{\eta_c} = 2980$ MeV). Recently the total $\gamma\gamma \to$ hadron cross section has been studied at LEP2 up to an invariant mass range of about 70 GeV [92]. We are concerned here mainly

with the invariant mass region relevant for RHIC and LHC (see the $\gamma\gamma$-luminosity figures below). Apart from the production of e^+e^- (and $\mu^+\mu^-$) pairs, the photons can always be considered as quasireal. The cross section section for virtual photons deviates from that for real photons only for Q^2, which are much larger then the coherence limit $Q^2 \lesssim 1/R^2$ (see also the discussion in [40]). For real photons general symmetry requirements restrict the possible final states, as is well known from the Landau–Yang theorem [93]. In particular, it is impossible to produce spin 1 final states. In e^+e^- annihilation, only states with $J^{PC} = 1^{--}$ can be produced directly. Two-photon collisions give access to most of the $C = +1$ mesons.

The cross section for $\gamma\gamma$-production in a heavy ion collision factorizes into a $\gamma\gamma$-luminosity function and a cross section $\sigma_{\gamma\gamma}(W_{\gamma\gamma})$ for the reaction of the (quasi)real photons $\gamma\gamma \to f$, where f is any final state of interest (see equation (25). When the final state is a narrow resonance, the cross section for its production in two-photon collisions is given by

$$\sigma_{\gamma\gamma\to R}(M^2) = 8\pi^2(2J_R + 1)\Gamma_{\gamma\gamma}(R)\delta(M^2 - M_R^2)/M_R \tag{68}$$

where J_R, M_R and $\Gamma_{\gamma\gamma}(R)$ are the spin, mass and two-photon width of the resonance R. This makes it easy to calculate the production cross section $\sigma_{AA\to AA+R}$ of a particle in terms of its basic properties. In figure 15 the function $4\pi^2 \mathrm{d}L_{\gamma\gamma}/\mathrm{d}M/M^2$ is plotted for various systems. It can be directly used to calculate the cross section for the production of a resonance R with the formula

$$\sigma_{AA\to AA+R}(M) = (2J_R + 1)\Gamma_{\gamma\gamma}\frac{4\pi^2\,\mathrm{d}L_{\gamma\gamma}/\mathrm{d}M}{M^2}. \tag{69}$$

We will now give a general discussion of possible photon–photon physics at relativistic heavy ion colliders. Invariant masses up to several GeV can be reached at RHIC and up to about 100 GeV at LHC.

We can divide our discussion into the following two main sections: basic QCD phenomena in $\gamma\gamma$-collisions (covering the range of meson, meson-pair production, etc) and $\gamma\gamma$-collisions as a tool for new physics, especially at very high invariant masses.

5.1. Basic QCD phenomena in $\gamma\gamma$-collisions

5.1.1. Hadron spectroscopy: light quark spectroscopy. One may say that photon–photon collisions provide an independent view of the meson and baryon spectroscopy. They provide powerful information on both the flavour and spin/angular momentum internal structure of

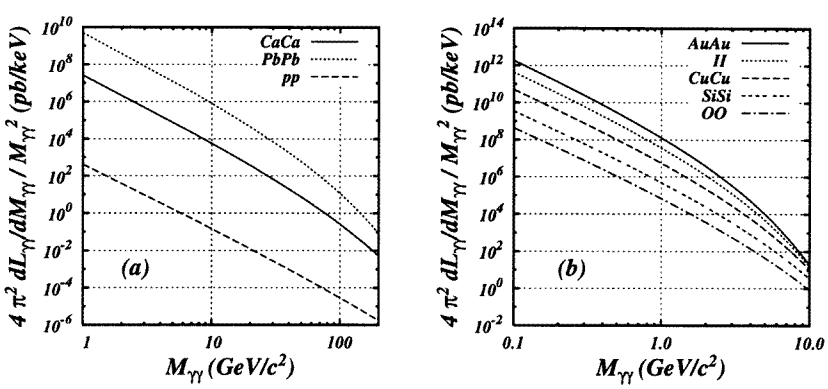

Figure 15. The universal function $4\pi^2 \mathrm{d}L_{\gamma\gamma}/\mathrm{d}M_{\gamma\gamma}/M_{\gamma\gamma}^2$ is plotted for different ion species at (*a*) LHC and (*b*) RHIC. For the parameters used see table 1.

the mesons. Much has already been done at e^+e^- colliders. For a review see, e.g. [94]. Light quark spectroscopy is very well possible at RHIC, benefiting from the high $\gamma\gamma$-luminosities. Detailed feasibility studies exist [18–21]. In this study, $\gamma\gamma$ signals and backgrounds from grazing nuclear and beam gas collisions were simulated with both the FRITIOF and VENUS Monte Carlo codes. The narrow $p_\perp$-spectra of the $\gamma\gamma$-signals provide a good discrimination against the background. The possibilities of the LHC are given in the FELIX LoI [23].

The absence of meson production via $\gamma\gamma$-fusion is also of great interest for glueball search. The two-photon width of a resonance is a probe of the charge of its constituents, so the magnitude of the two-photon coupling can serve to distinguish quark dominated resonances from glue-dominated resonances ('glueballs'). In $\gamma\gamma$-collisions, a glueball can only be produced via the annihilation of a $q\bar{q}$ pair into a pair of gluons, whereas a normal $q\bar{q}$-meson can be produced directly, so we estimate

$$\frac{\sigma(\gamma\gamma \to M)}{\sigma(\gamma\gamma \to G)} = \frac{\Gamma(M \to \gamma\gamma)}{\Gamma(G \to \gamma\gamma)} \sim \frac{1}{\alpha_s^2} \tag{70}$$

where α_s is the strong interaction coupling constant and where G is a 'glueball', M a normal $q\bar{q}$-meson. Glueballs are produced most easily in a gluon-rich environment. This is, e.g. the case in radiative J/Ψ decays, $J/\Psi \to \gamma gg$.

In order to form a meson out of the gluon pair, they must first annihilate into a $q\bar{q}$ pair. So we estimate

$$\frac{\Gamma(J/\Psi \to \gamma G)}{\Gamma(J/\Psi \to \gamma M)} \sim \frac{1}{\alpha_s^2}. \tag{71}$$

The 'stickiness' of a mesonic state is defined as (see, e.g. [95])

$$S_X = \frac{\Gamma(J/\Psi \to \gamma X)}{\Gamma(J/\Psi \to \gamma\gamma)}. \tag{72}$$

We expect the stickiness of all mesons to be comparable, while for glueballs it should be enhanced by a factor of about $S_{\mathrm{G}}/S_{\mathrm{M}} \approx 1/\alpha_s^4 \sim 20$.

Recently in [96] results of the search for $f_J(2220)$ production in two-photon interactions were presented. There a very small upper limit for the product of $\Gamma_{\gamma\gamma} B_{K_s K_s}$ was given, where $B_{K_s K_s}$ denotes the branching fraction of its decay into $K_s K_s$. From this it was concluded that this is a strong evidence that the $f_J(2220)$ is a glueball.

5.1.2. Heavy quark spectroscopy. For charmonium production, the two-photon width $\Gamma_{\gamma\gamma}$ of η_c (2960 MeV, $J^{PC} = 0^{-+}$) is known from experiment, but the two-photon widths of P-wave charmonium states have been measured with only modest accuracy. For RHIC the study of η_c is a real challenge [19]; the luminosities are falling and the branching ratios to experimentally interesting channels are small.

In table 3 (adapted from table 2.6 of [23]) the two-photon production cross sections for $c\bar{c}$ and $b\bar{b}$ mesons in the rapidity range $|Y| < 7$ are given. Also given are the number of events in a 10^6 s run with the ion luminosities of 4×10^{30} cm^{-2} s^{-1} for Ca–Ca and 10^{26} cm^{-2} s^{-1} for Pb–Pb. Millions of C-even charmonium states will be produced in coherent two-photon processes during a standard 10^6 s heavy ion run at the LHC. The detection efficiency of charmonium events has been estimated as 5% for the forward–backward FELIX geometry [23], i.e. one can expect detection of about 5×10^3 charmonium events in Pb–Pb and about 10^6 events in Ca–Ca collisions. This is two to three orders of magnitude higher than what is expected during five years of LEP200 operation. Further details, also on experimental cuts, backgrounds and the possibilities for the study of C-even bottonium states are given in [23].

Table 3. Production cross sections and event numbers for heavy quarkonia produced in a 10^6 s run in Pb–Pb and Ca–Ca collisions at the LHC with luminosities 10^{27} and 4×10^{30} cm^{-2} s^{-1}. Adapted from [23].

State	Mass MeV	$\Gamma_{\gamma\gamma}$ keV	$\sigma(AA \to AA + X)$ Pb–Pb	Ca–Ca	Events for 10^6 s Pb–Pb	Ca–Ca
η'	958	4.2	22 mbarn	125 μbarn	2.2×10^7	5.0×10^8
η_c	2981	7.5	590 μbarn	3.8μbarn	5.9×10^5	1.5×10^7
χ_{0c}	3415	3.3	160 μbarn	1.0 μbarn	1.6×10^5	4.0×10^6
χ_{2c}	3556	0.8	160 μbarn	1.0 μbarn	1.6×10^5	4.0×10^6
η_b	9366	0.43	370 nbarn	3.0 nbarn	370	12 000
η_{0b}	9860	2.5×10^{-2}	18 nbarn	0.14 nbarn	18	640
η_{2b}	9913	6.7×10^{-3}	23 nbarn	0.19 nb	23	76

5.1.3. Vector meson pair production. Total hadronic cross section. There are various mechanisms to produce hadrons in photon–photon collisions. Photons can interact as point particles which produce quark–antiquark pairs (jets) (see figure 16(*a*)), which subsequently hadronize. Often a quantum fluctuation transforms the photon into a vector meson (ρ,ω,ϕ, ...) (VMD component) opening up all the possibilities of hadronic interactions (figure 16(*b*)). In hard scattering, the structure of the photon can be resolved into quarks and gluons. Leaving a spectator jet, the quarks and gluon contained in the photon will take part in the interaction, some examples are given in figures 16(*c*) and (*d*). It is of great interest to study the relative amounts of these components and their properties.

The L3 collaboration recently made a measurement of the total hadron cross section for photon–photon collisions in the interval 5 GeV $< W_{\gamma\gamma} <$ 75 GeV [92]. It was found that the $\gamma\gamma \to$ hadrons cross section is consistent with the universal Regge behaviour of total hadronic cross sections. They show a steep decrease in the region of low centre-of-

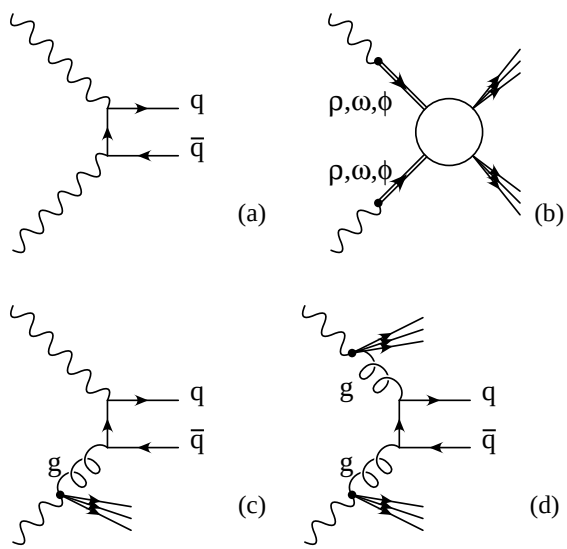

Figure 16. Diagrams showing the contribution to the $\gamma\gamma \to$ hadron reaction: (*a*) direct mechanism, (*b*) vector meson dominance, (*c*) single and (*d*) double resolved photons.

mass energy followed by a slow rise at high energies. It is parametrized as follows (see equation (5) of [92])

$$\sigma_{\rm tot} = A(s/s_0)^{\epsilon} + B(s/s_0)^{-\eta} \tag{73}$$

with $\epsilon = 0.0790 \pm 0.0011$, $\eta = 0.4678 \pm 0.0059$, $A = 173 \pm 7$ nbarn, $B = 519 \pm 125$ nbarn, and $s_0 = 1$ GeV^2. Using this together with the effective luminosities (see table 1), one expects about 3×10^6 events GeV^{-1} at an invariant mass of 25 GeV and still 4×10^4 events GeV^{-1} at $W_{\gamma\gamma} = 100$ GeV.

The production of vector meson pairs can be studied at RHIC with high statistics in the GeV region [18]. For the possibilities at LHC, we refer the reader to [23, 24], where experimental details and simulations are also described.

5.2. $\gamma\gamma$-collisions as a tool for new physics

The high flux of photons at relativistic heavy ion colliders offers possibilities for the search of new physics. This includes the discovery of the Higgs boson in the $\gamma\gamma$-production channel or new physics beyond the standard model, such as supersymmetry or compositeness.

Let us mention here the plans to build a e^+e^- linear collider. Such future linear colliders will be used for e^+e^-, $e\gamma$ and $\gamma\gamma$-collisions (PLC, photon linear collider). The photons will be obtained by the scattering of laser photons (of eV energy) on high-energy electrons ($\approx$ TeV region) (see [97]). Such photons in the TeV energy range will be monochromatic and polarized. The physics programme at such future machines is discussed in [98], it includes Higgs boson and gauge boson physics and the discovery of new particles.

While the $\gamma\gamma$-invariant masses which will be reached at RHIC will mainly be useful to explore QCD at lower energies, the $\gamma\gamma$-invariant mass range at LHC—up to about 100 GeV—will open up new possibilities.

A number of calculations have been made for a medium heavy standard model Higgs [99–102]. For masses $m_{\rm H} < 2m_{\rm W^\pm}$ the Higgs bosons decays dominantly into $b\bar{b}$, whereas a heavier Higgs decays into a W^+W^- pair. For the $\gamma\gamma \to$ H cross section we can use equation (69), where the two-photon width of the Higgs bosons in the standard model can be found, e.g. in [99]. The calculations, using the integrated luminosity of table 1, show that for Ca–Ca collisions only about one Higgs boson is produced during one year of the LHC operation. Therefore, the chances of finding the standard model Higgs in this case are marginal [24].

An alternative scenario with a light Higgs boson was, e.g. given in [103] in the framework of the 'general two-Higgs doublet model'. Such a model allows for a very light particle in the few GeV region. With a mass of 10 GeV, the $\gamma\gamma$-width is about 0.1 keV (see figure 1 of[103]). We get 2×10^3 events for Ca–Ca collisions, 40 for pp and 8 for Pb–Pb, with the integrated luminosities of table 1. The authors of [103] proposed to look for such a light neutral Higgs boson at the proposed low-energy $\gamma\gamma$-collider. We want to point out that the LHC Ca–Ca heavy ion mode would also be very suitable for such a search.

One can also speculate about new particles with strong coupling to the $\gamma\gamma$-channel. Large $\Gamma_{\gamma\gamma}$-widths will directly lead to large $\gamma\gamma$-production cross sections, see equation (69). We quote the papers [104, 105]. Since the $\gamma\gamma$-width of a resonance is mainly proportional to the wavefunction at the origin, huge values can be obtained for very tightly bound systems. Composite scalar bosons at $W_{\gamma\gamma} \approx 50$ GeV are expected to have $\gamma\gamma$-widths of several MeV [104, 105]. The search for such resonances in the $\gamma\gamma$-production channel will be possible at LHC. Production cross section can be directly read off from equation (69) and figure 15.

For example, take $W_{\gamma\gamma} = 50$ GeV and assume a width of $\Gamma_{\gamma\gamma} = 1$ MeV, one obtains for a scalar particle ($J_R = 0$) $\sigma_{\mathrm{CaCa}} \approx 1$ MeV10 pb keV^{-1} = 10 nbarn. With an integrated luminosity of 4 pbarn^{-1} in the Ca–Ca mode, one obtains 4×10^4 events.

In [59, 60] $\gamma\gamma$-processes at pp colliders (LHC) are studied. It is observed there that non-strongly interacting supersymmetric particles (sleptons, charginos, neutralinos, and charged Higgs bosons) are difficult to detect at the LHC. The Drell–Yan and gg-fusion mechanisms yield low production rates for such particles. Therefore the possibility of producing such particles in $\gamma\gamma$-interactions at hadron colliders is examined. Since photons can be emitted from protons which do not break up in the radiation process (see also section 3) clean events can be generated which should compensate for the small number. Formulae and graphs for the production of supersymmetric particles are also given in [16], where further references can also be found.

In [59] it was pointed out that at the high luminosity of $L = 10^{34}$ cm^{-2} s^{-1} at the LHC(pp), one expects about 16 minimum bias events per bunch crossing. Even the elastic $\gamma\gamma$ events will therefore not be free of hadronic debris. Clean elastic events will be detectable at luminosities below 10^{33} cm^{-2} s^{-1}. This danger of 'overlapping events' has also to be checked for the heavy ion runs, but it will be much reduced owing to the lower luminosities.

Detailed calculations have also been made for the production of a charged chargino pair via $\gamma\gamma \to \tilde{\chi}_1^+ \tilde{\chi}_1^-$. The production of these charginos can be studied via their decay into a neutralino and a fermion–antifermion pair. $\tilde{\chi}_1^\pm \to \tilde{\chi}_1^0 f_i \bar{f}_j$. The most clean channel is into muons or electrons. Such an event would therefore be characterized by two fermions of opposite charge (e^+e^-, $\mu^+\mu^-$ or $e^\pm\mu^\mp$) together with an unbalanced transverse momentum. In order to be able to detect the missing momentum, a closed geometry is needed. Studies were made for this process as a function of the mass of the chargino. In this case the main background—the production of a W^+W^- pair also decaying into two leptons of opposite charge—was studied also. The cross section for this process was found to be 3.6 pbarn, comparable to the chargino pair production. However, the harder momentum distribution of this background process can be used to distinguish it from the chargino production. Similar calculations have also been made for pp collisions [60].

6. Diffractive processes as background

Diffractive processes are an important class of background to $\gamma\gamma$ final states. As the nuclei can remain intact in these collisions, they have the same signature as the photon–photon events. Therefore they cannot be distinguished from each other. Diffractive events have been studied extensively at HERA for photon-proton collisions. A future programme will also study diffractive processes involving nuclei [106]. Diffraction processes in pp and $p\bar{p}$ are also well known from studies at the Tevatron and ISR (CERN).

Diffractive events at high energies are best described within Regge theory and in the language of the Pomeron (see, e.g. [107]). It is needless to say that the possibility to study photon–Pomeron and also Pomeron–Pomeron collisions in peripheral collisions are interesting fields in themselves. In particular, photon–Pomeron fusion processes could be of interest, as they allow for final states, which are not directly possible in photon–photon events (see also the discussion about the diffractive vector meson production in γA collisions in section 4). Here we restrict ourselves to the estimate, how big the contribution of diffractive processes are compared with photon–photon events. Of course it is difficult to give quantitative answers at present.

A number of calculations were made within the phenomenological dual parton model (DPM) [108]. These calculations [108] have been interpreted, that Pomeron–Pomeron fusion dominates over the photon–photon cross section for almost all ions used. Only for the very heavy ions, such as Pb–Pb, does the photon–photon process become comparable. Unfortunately these calculations were made without the constraint that the nuclei remain intact in the final state. As the nuclei are only a weakly bound system and the nuclear interaction strong, it is very likely that a short-range interaction between them leads to the break-up of the nucleus. More refined calculations have been made in the meantime [109]. The cross sections for diffractive processes are then reduced by roughly two orders of magnitude for Ca–Ca and three orders of magnitude for Pb–Pb (both at LHC conditions). Only for proton–proton collisions can diffractive processes be expected to dominate over photon–photon ones. Particle production from diffractive processes are also studied in [110, 111]. They also find that the increase of the cross section with mass number A is much smaller than that for electromagnetic processes.

The problem of separating two-photon signals from the background has been studied in detail for RHIC conditions in [112]. Four sources of background have been considered: peripheral (hadronic) nucleus–nucleus collisions, beam–gas interactions, gamma–nucleus interactions and cosmic rays. In order to separate signals from background, cuts have been developed which utilize the characteristics of two-photon interactions; the most important of these cuts are multiplicity and transverse momentum. It was shown in [4], to which we refer the reader for details, that there are high rates of $\gamma\gamma$-interactions and that the signals can well be separated from the background.

7. Electron–positron pair production and QED of strong fields

Electrons (positrons) and to some extent also muons have a special status, which is due to their small mass. They are therefore produced more easily than other heavier particles and in the case of e^+e^- pair production lead to new phenomena, such as multiple pair production. In addition the Compton wavelength of the electron (≈ 386 fm) is much larger than the size of the nuclei ($\gtrsim 7$ fm). This also means that the virtuality Q^2 of the photons, which ranges from 0 up to the order of $1/R^2$ can be much larger than the electron mass m_e^2. Whereas in all cases discussed above we could treat the photons as being quasireal and relate their cross section to the photon cross section; here this is no longer the case in general and therefore corrections to the EPA are needed.

The muon has a Compton wavelength of about 2 fm. This length is of the same order as the nuclear radius. We therefore expect that the EPA will give more reliable results. Both electrons and muons can be produced not only as free particles but also into an atomic state bound to one of the ions.

7.1. Free pair production, strong field effects and multiple pair production

We consider the e^+e^- pair production in the collision of two nuclei with charges Z_1 and Z_2 and relative velocity v. For $v \to 0$ the electrons and positrons can adjust adiabatically to the motion of the nuclei and, with sufficiently high charge Z_1 and Z_2 one can enter a supercritical regime, where $(Z_1 + Z_2)\alpha > 1$. Such a situation has been studied extensively at GSI and later at Argonne; we refer the reader to the (vast) literature on this subject, see [113] where further references are given. We here study the opposite region, with $v \approx c$. A very useful and complete reference for this field is [114].

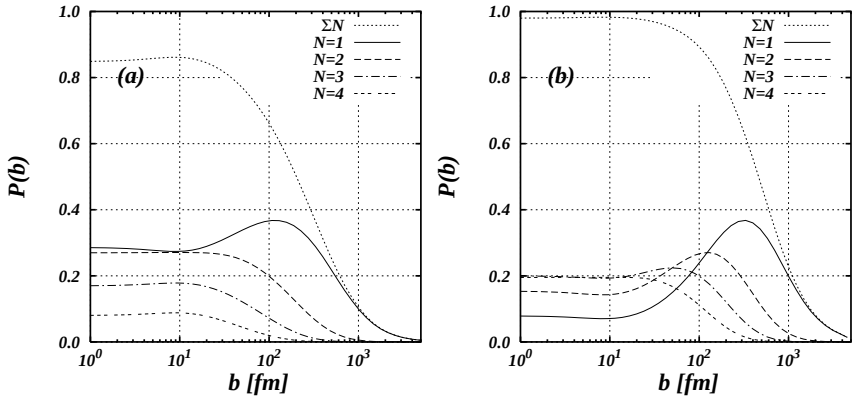

Figure 17. The impact-parameter dependent probability to produce N e^+e^- pairs ($N = 1, 2, 3, 4$) in one collision is shown for both RHIC (a, $\gamma = 106$, Au–Au) and LHC (b, $\gamma = 2950$, Pb–Pb). Also shown is the total probability to produce at least one e^+e^- pair. One sees that at small impact parameters multiple pair production can be dominant over single pair production.

The special situation of the electron pairs can already be seen from the formula for the impact-parameter dependent probability in lowest order. Using EPA one obtains [1]

$$P^{(1)}(b) \approx \frac{14}{9\pi^2}(Z\alpha)^4 \frac{1}{m_e^2 b^2} \ln^2\left(\frac{\gamma\delta}{2m_e b}\right) \tag{74}$$

where $\delta \approx 0.681$ and $\gamma = 2\gamma_{cm}^2 - 1$ the Lorentz factor in the target frame, one can see that at RHIC and LHC energies and for impact parameters of the order of the Compton wavelength $b \approx 1/m_e$, this probability exceeds one. It was first described in [115] how unitarity can be restored by considering the production of multiple pairs†.

Multiple pair production was later studied by a number of authors [108–111] using different approximations. A general feature found by all was the fact that the probability is given to a good approximation by a Poisson distribution:

$$P(N, b) \approx \frac{[P^{(1)}(b)]^N}{N!} \exp[-P^{(1)}(b)] \tag{75}$$

where $P^{(1)}(b)$ is the single pair creation probability from perturbation theory, see, e.g. equation (74). Deviations from this Poisson form were studied in [120] and were found to be small at high energies.

The impact-parameter dependence of the lowest order process was calculated in [121, 122] (see also figure 17), the total cross section for the one-pair production in [123], for one and multiple pair production in [124] (see figure 18). Of course the total cross section is dominated by the single pair production as the main contribution to the cross section comes from very large impact parameters b. On the other hand one can see that for impact parameters b of about $2R$ the number of electron–positron pairs produced in each ion collision is about 5 (2) for LHC with $Z = 82$ (RHIC with $Z = 79$). This means that each photon–photon event—especially those at a high invariant mass—which occur predominantly at impact parameters close to $b \gtrsim 2R$—is accompanied by the production of several (low-energy) e^+e^- pairs.

† It is interesting to remark that the fact that pair production in ion collisions grows beyond the unitarity limit was already observed by Heitler [116]. Of course at that time available energies made this only 'of academic interest'.

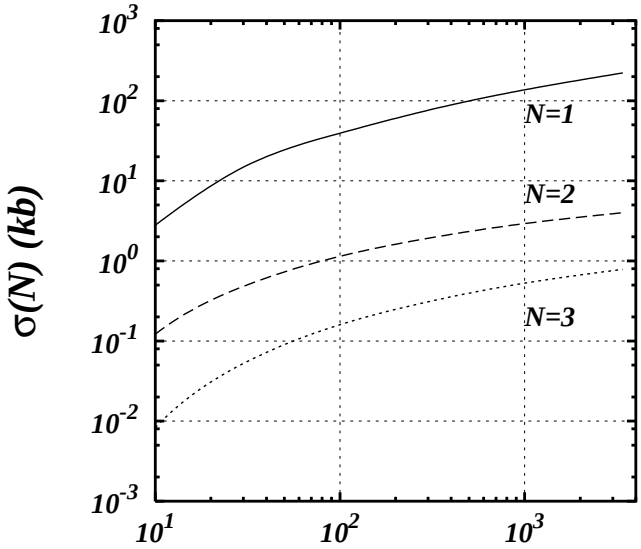

Figure 18. The total cross sections for the multiple pair production of up to three pairs are shown as a function of the Lorentz factor γ. Shown are the results for a Pb–Pb collision.

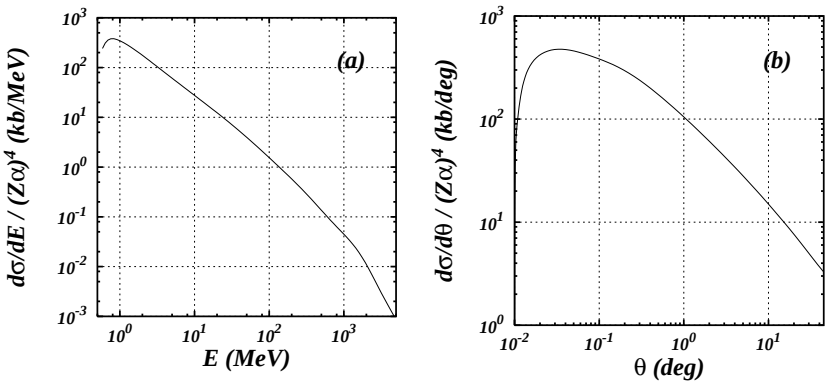

Figure 19. The single differential cross section for e^+e^- pair production at LHC energies. Shown are the cross sections as a function of (*a*) the energy of either electron or positron, and (*b*) as a function of the angle with the beam axis θ.

As the total cross section for this process is huge (about 200 kbarn for Pb at LHC, 30 kbarn for Au at RHIC), one has to take this process into account as a possible background process. Most of the particles are produced at low invariant masses (below 10 MeV) and into the very forward direction (see figure 19). Therefore most of them leave the detector along the beam pipe and are not observed. On the other hand a substantial amount of them is left also at high energies, e.g. above 1 GeV. These QED pairs also constitute a potential hazard for detectors at the colliders. In table 4 we show the cross section for this process with the energy of either the electron or the positron above a certain threshold. Singles angular distributions of electrons (positrons) are calculated for peripheral collisions using EPA in [125]. Numerical results in the relevant energy and angular ranges are presented there. The physics is discussed in terms of easy to handle analytical formulae.

Table 4. The cross sections of e^+e^- pair production with *both* electron and positron having an energy above a certain threshold value. Shown are results for both LHC for two different ion species.

$E_{\rm thr}$ (GeV)	σ (Pb–Pb, LHC)	σ (Ca–Ca, LHC)
0.25	3.5 kbarn	12 barn
0.50	1.5 kbarn	5.5 barn
1.0	0.5 kbarn	1.8 barn
2.5	0.08 kbarn	0.3 barn
5.0	0.03 kbarn	0.1 barn

Differential production probabilities for $\gamma\gamma$-dileptons in central relativistic heavy ion collisions are calculated using EPA and an impact-parameter formulation and compared with the Drell–Yan and thermal ones in [45, 126, 127]. The very low $p_\perp$ values and the angular distribution of the pairs give an idea of their discrimination. Nuclear stopping leads to bremsstrahlung pair production and some modification of the $\gamma\gamma$-dilepton spectra. For details we refer the reader to these references. In [128] the low-energy dilepton spectrum in 16 GeV π–p collisions was studied using the two-photon mechanism. It was found that this mechanism could not explain the experimental data [129]. This is in contrast to the findings of [130].

In the Bethe–Heitler process $\gamma + Z \to e^+e^- + Z$ higher order effects are well known. Using Sommerfeld–Maue wavefunctions higher order effects are taken into account. This leads to a modification of the Born result. For example, the total cross section (no screening) for $\omega \gg m_e$ is given by (see [131])

$$\sigma = \frac{28}{9} Z^2 \alpha r_e^2 \left[\ln \frac{2\omega}{m_e} - \frac{109}{42} - f(Z\alpha) \right] \tag{76}$$

with the higher order term given by

$$f(Z\alpha) = (Z\alpha)^2 \sum_{n=1}^{\infty} \frac{1}{n(n^2 + (Z\alpha)^2)} \tag{77}$$

and $r_e = \alpha/m_e$ is the classical electron radius. As far as total cross sections are concerned the higher order contributions tend to a constant.

Using those results a modification of e^+e^- pair creation in $Z_1 + Z_2$ collisions with respect to the lowest order result was obtained [1]. Such a treatment was not symmetrical with respect to Z_1 and Z_2 and an *ad hoc* symmetrization was introduced there (see equation (7.3.7) of [1]).

A systematic way to take leading terms of higher order effects into account in e^+e^- pair production is pursued in [132] using Sudakov variables and the impact-factor representation.

Non-perturbative effects are also studied in a light-front approach [133]. In this approach a gauge transformation on the time-dependent Dirac equation is performed, in order to remove the explicit dependence on the long-range part of the interaction. Similar approaches are also studied in [134, 135]. Numerical evaluation of the non-perturbative effects will be considered in a future work.

In this context the paper [136] is of interest. In this work the electromagnetic field of a particle with velocity v is calculated, see e.g. the textbook result of [30]. Then the limit $v \to c$ is performed. This corresponds to the electromagnetic fields of a massless particle, which can be regarded as an 'electromagnetic shock wave'. The results of this

paper are very much reminiscent of the sudden approximation in the semiclassical theory; for a connection of semiclassical and eikonal methods see also [137].

7.2. Bound–free pair production

The bound–free pair production, also known as electron-pair production with capture, is a process which is also of practical importance in the collider. It is the process where a pair is produced but with the electron not as a free particle, but into an atomic bound state of one of the nuclei. As this changes the charge state of the nucleus, it is lost from the beam. Together with the electromagnetic dissociation of the nuclei (see section 4) these two processes are the dominant loss processes for heavy ion colliders.

In [1] an approximate value for this cross section is given as

$$\sigma_{\mathrm{capt}}^{K} \approx \frac{33\pi}{10} Z_1^2 Z_2^6 \alpha^6 r_{\mathrm{e}}^2 \frac{1}{\exp(2\pi Z_2 \alpha) - 1} \left[\ln(\gamma\delta/2) - \frac{5}{3} \right] \tag{78}$$

where only capture to the K-shell is included. The cross section for all higher shells is expected to be of the order of 20% of this cross section (see equations 7.6.23 and 24 of [1]).

The cross section in equation (78) is of the form

$$\sigma = A \ln \gamma + B. \tag{79}$$

This form has been found to be a universal one at sufficiently high values of γ. The constant A and B then only depend on the type of the target.

The above cross section was found making use of the EPA and also using an approximate wavefunction for bound state and continuum. More precise calculations exist [127–132] in the literature. Recent calculations within PWBA for high values of γ have shown that the exact first-order results do not differ significantly from EPA results [144, 145]. Parametrizations for A and B [139, 141] for typical cases are given in table 5.

For a long time the effect of higher order and non-perturbative processes has been under investigation. At lower energies, in the region of a few GeV per nucleon, coupled-channel calculations have indicated for a long time, that these give large contributions, especially at small impact parameters. Newer calculation tend to predict considerably smaller values, of the order of the first-order result and in a recent article Baltz [146] finds in the limit $\gamma \to \infty$ that contributions from higher orders are even slightly smaller than the first-order results.

The bound–free pair production was measured in two recent experiments at the SPS, at $\gamma = 168$ [147] and at $\gamma \approx 2$ [148, 149]. Both experiments found good agreement between measurement and calculations.

A similar process was recently used at LEAR (CERN) to produce antihydrogen. An antiproton beam with a momentum of 1.94 GeV/c hit a Xenon target ($Z = 54$) to produce and detect antihydrogen in the bound–free pair production mechanism[150]. The same

Table 5. Parameters A and B (see equation (79)) as well as total cross sections for the bound–free pair production for RHIC and LHC. The parameters are taken from [141].

Ion	A	B	σ(Au, $\gamma = 106$)	σ(Pb, $\gamma = 2950$)
Pb	15.4 barn	−39.0 barn	115 barn	222 barn
Au	12.1 barn	−30.7 barn	90 barn	173 barn
Ca	1.95 mbarn	−5.19 mbarn	14 mbarn	27.8 mbarn
O	4.50 μbarn	−12.0 μbarn	32 μbarn	64.3 μbarn

technique is also used at Fermilab [151], where it is also planned to measure the Lamb shift in antihydrogen as a test of CPT invariance [152, 153]. Their results are in good agreement with the recent calculations [144, 145].

We note that the electron and positron can also form a bound state, positronium. This is in analogy to the $\gamma\gamma$-production of mesons ($q\bar{q}$ states) discussed in section 5. With the known width of the parapositronium $\Gamma((e^+e^-)_{n=1}{}^1S_0 \to \gamma\gamma) = mc^2\alpha^5/2$, the photon–photon production of this bound state was calculated in [154]. The production of orthopositronium, $n = 1\,{}^3S_1$ was calculated recently [77].

As discussed in section 5 the production of orthopositronium is only suppressed by the factor $(Z\alpha)^2$, which is not very small. Therefore one expects that both kinds of positronium are produced in similar numbers. Detailed calculation show that the three-photon process is indeed not much smaller than the two-photon process [77, 81].

8. Conclusion

In this review the basic properties of electromagnetic processes in very peripheral hadron–hadron collisions (we deal mainly with nucleus–nucleus collisions, but proton–proton collisions are also treated) are described. The method of equivalent photons is a well established tool to describe these kind of reactions. Reliable results of quasireal photon fluxes and $\gamma\gamma$-luminosities are available. Unlike electrons and positrons heavy ions are particles with an internal structure. We have described how to treat effects arising from this structure, and we conclude that such effects are well under control. A problem, which is difficult to judge quantitatively at the moment, is the influence of strong interactions in grazing collisions, i.e. effects arising from the nuclear stratosphere and Pomeron interactions.

The high photon fluxes open up possibilities for photon–photon as well as photon–nucleus interaction studies up to energies hitherto unexplored at the forthcoming colliders RHIC and LHC. Interesting physics can be explored at the high invariant $\gamma\gamma$-masses, where detecting new particles could be within range. Also very interesting studies within the standard model, i.e. mainly QCD studies will be possible. This ranges from the study of the total $\gamma\gamma$-cross section into hadronic final states up to invariant masses of about 100 GeV to the spectroscopy of light and heavy mesons.

We also reviewed dilepton production in very peripheral collisions. This is essentially well understood and gives rise to an experimental background. Multiple pair production is a strong-field effect of principle interest. Pair production with capture is, in addition to nuclear fragmentation (sometimes called the 'Weizsäcker–Williams process'), a source of beam loss in the collider operation.

RHIC will be operational in only one year, LHC in approximately seven years. Therefore the planning of the experiments and necessary detectors for this kind of physics has to be done now. With the new data and new insights, that will come from these experiments, new work and theoretical understanding will be required. As an ancient motto says: 'no surprise would be a surprise'.

Acknowledgments

We have benefited from numerous discussions with many people over the past years. We thank all of them, especially we wish to mention A Alscher, N Baron, C A Bertulani, I Ginzburg, O Conradt, S Datz, K Eggert, R Engel, S Gevorkyan, M Greiner, Z Halabuka, S Klein, F Krauss, H Meier, N N Nikolaev, S Sadovsky, R Schuch and G Soff.

References

[1] Bertulani C A and Baur G 1988 *Phys. Rep.* **163** 299
[2] Baur G and Rebel H 1994 *J. Phys. G: Nucl. Part. Phys.* **20** 1
[3] Baur G and Rebel H 1996 *Ann. Rev. Nucl. Part. Sci.* **46** 321
[4] Primakoff H 1951 *Phys. Rev.* **31** 899
[5] Moshammer R *et al* 1997 *Phys. Rev. Lett.* **79** 3621
[6] Landau L D and Lifshitz E M 1934 *Phys. Z. Sowjet.* **6** 244
[7] Soff G 1980 *Proc. 18th Winter School (Bielsko-Biala, Poland)* ed A Balanda and Z Stachura p 201
[8] Alexander G, Gotsman E and Maor U 1987 *Z. Phys.* C **34** 329
[9] Baur G and Bertulani C A 1988 *Z. Phys.* A **330** 77
[10] Grabiak M, Müller B, Greiner W and Koch P 1989 *J. Phys. G: Nucl. Part. Phys.* **15** L25
[11] Papageorgiu E 1989 *Phys. Rev.* D **40** 92
[12] Baur G 1990 *CBPF Int. Workshop on Relativistic Aspects of Nuclear Physics (Rio de Janeiro, Brazil, 1989)* ed T Kodama *et al* (Singapore: World Scientific) p 127
[13] Baur G and Ferreira Filho L G 1990 *Nucl. Phys.* A **518** 786
[14] Cahn N and Jackson J D 1990 *Phys. Rev.* D **42** 3690
[15] Vidović M, Greiner M, Best C and Soff G 1993 *Phys. Rev.* C **47** 2308
[16] Krauss F, Greiner M and Soff G 1997 *Prog. Part. Nucl. Phys.* **39** 503
[17] Vannucci F 1980 *$\gamma\gamma$ Collisions, Proc., (Amiens 1980)* (*Lect. Notes Phys.* **134**) ed G Cochard (Berlin: Springer)
[18] Klein S and Scannapieco E 1997 *Photon '97, Egmond aan Zee* ed A Buis (Singapore: World Scientific) p 369
[19] Klein S and Scannapieco E 1997 Coherent photons and pomerons in heavy ion collisions *6th Conf. on the Intersections of Particle and Nuclear Physics, (Big Sky, Montana)* STAR Note 298, LBNL-40495
[20] Klein S and Scannapieco E 1995 STAR Note 243
[21] Klein S 1995 *Photon '95, Sheffield* ed D J Miller *et al* (Singapore: World Scientific) p 417
[22] Hencken K, Kharlov Yu V, Khaustov G V, Sadovsky S A and Samoylenko V D 1996 *TPHIC, Event Generator Of Two Photon Interactions in Heavy Ion Collisions* IHEP-96-38
[23] Eggert K *et al* 1997 *FELIX Letter of Intent* CERN/LHCC 97–45, LHCC/I10
[24] Baur G, Hencken K, Trautmann D, Sadovsky S and Kharlov Yu 1998 *Photon–Photon Physics With Heavy Ions at CMS* CMS Note 1998/009, available from the CMS information server at http://cmsserver.cern.ch
[25] Block M M and Cahn R 1985 *Rev. Mod. Phys.* **57** 563
[26] Abe F *et al* 1994 *Phys. Rev.* D **50** 5550
[27] Abe F *et al* 1994 *Phys. Rev.* D **50** 5535
[28] Abe F *et al* 1994 *Phys. Rev.* D **50** 5518
[29] Greider K R 1965 *Ann. Rev. Nucl. Part. Sci.* **15** 291
[30] Jackson J D 1975 *Classical Electrodynamics* (New York: Wiley)
[31] Nörenberg W and Weidenmüller H A 1980 *Introduction to the Theory of Heavy Ion Collisions* (Berlin: Springer)
[32] Frahn W E 1972 *Ann. Phys.* **72** 524
[33] Barnett R M *et al* 1996 *Phys. Rev.* D **54** 1
[34] Kopeliovich B Z, Nikolaev N N and Potashnikova I K 1988 *Phys. Rev.* D **39** 769
[35] Glauber R J 1967 *High Energy Physics and Nuclear Structure* (Amsterdam: North-Holland) p 311
[36] Engel J, Gaisser T K, Lipari P and Stanev T 1992 *Phys. Rev.* D **46** 5013
[37] Bertsch G, Brown B A and Sagawa H 1989 *Phys. Rev.* C **39** 1154
[38] Abbiendi G 1997 *Nuovo Cimento* **20** 1
[39] Engel R 1997 *PhD Thesis* Universität Gesamthochschule Siegen
[40] Budnev V M, Ginzburg I F, Meledin G V and Serbo V G 1975 *Phys. Rep.* **15** 181
[41] Winther A and Alder K 1979 *Nucl. Phys.* A **319** 518
[42] Abramowitz M and Stegun I A 1965 *Handbook of Mathematical Functions* (New York: Dover)
[43] Baur G and Ferreira Filho L G 1991 *Phys. Lett.* B **254** 30
[44] Baur G and Baron N 1993 *Nucl. Phys.* A **561** 628
[45] Baur G 1992 *Z. Phys.* C **54** 419
[46] Baron N and Baur G 1994 *Phys. Rev.* C **49** 1127
[47] Vidović M, Greiner M and Soff G 1993 *Phys. Rev.* C **48** 2011
[48] Baltz A J, Rhoades-Brown M J and Weneser J 1996 *Phys. Rev.* E **54** 4233
[49] Baltz A J and Strikman M 1998 *Phys. Rev.* D **57** 548

[50] Baltz A, Chasman C and White S N 1998 *Preprint* nucl-ex/9801002
[51] Hencken K, Trautmann D and Baur G 1996 *Phys. Rev.* C **53** 2532
[52] Hencken K, Trautmann D and Baur G 1995 *Z. Phys.* C **68** 473
[53] Conradt O 1996 *Diplomarbeit* Universität Basel (unpublished)
[54] Kniehl B 1991 *Phys. Lett.* B **254** 267
[55] Chanfray G, Delorme J, Ericson M and Molinari A 1993 *Nucl. Phys.* A **556** 439
[56] Baron N 1994 *PhD Thesis* Forschungszentrum Jülich, Institut für Kernphysik Jül-2846
[57] deForest T and Walecka J D 1966 *Adv. Phys.* **15** 1
[58] Halzen F and Martin A D 1984 *Quarks & Leptons* (New York: Wiley)
[59] Drees M, Godbole R M, Nowakowski N and Rindami S D 1994 *Phys. Rev.* D **50** 2335
[60] Ohnemus J, Walsh T F and Zerwas P M 1994 *Phys. Lett.* B **328** 369
[61] Martin A D *et al* 1993 *Phys. Lett.* B **306** 306
[62] Martin A D *et al* 1993 *Phys. Lett.* B **309** 492
[63] Bauer T H, Spital R D, Yennie D R and Pipkin F M 1978 *Rev. Mod. Phys.* **50** 261
[64] Norbury J W and Waldsmith M 1998 *Phys. Rev.* C **57** 1525
[65] Brechtmann C and Heinrich W 1988 *Z. Phys.* A **330** 407
[66] Brechtmann C and Heinrich W 1988 *Z. Phys.* A **331** 463
[67] Price P B, Guaxiao R and Williams W T 1988 *Phys. Rev. Lett.* **61** 2193
[68] Pshenichnov I A *et al* 1998 *Phys. Rev.* C **57** 1920
[69] Baur G and Bertulani C A 1989 *Nucl. Phys.* A **505** 835
[70] Datz S *et al* 1997 *Phys. Rev. Lett.* **79** 3355
[71] Norbury J W and Baur G 1993 *Phys. Rev.* C **48** 1915
[72] Crittenden J A 1997 Exclusive production of neutral vector mesons at the electron-proton collider HERA *Springer Tracts in Modern Physics* vol 140 (Heidelberg: Springer)
[73] Ryskin M G, Roberts R G, Martin A D and Levin E M 1997 *Z. Phys.* C **76** 231
[74] Breitweg J *et al* 1997 *Z. Phys.* C **76** 599
[75] Miller D J 1998 *J. Phys. G: Nucl. Part. Phys.* **24** 317
[76] Freedman D Z, Schramm D N and Tubbs D L 1977 *Ann. Rev. Nucl. Part. Sci.* **27** 167
[77] Ginzburg I F private communication
[78] Ginzburg I F *et al* 1987 *Nucl. Phys.* B **284** 685
[79] Ginzburg I F *et al* 1988 *Nucl. Phys.* B **296** 569
[80] Ginzburg I F *et al* 1992 *Nucl. Phys.* B **388** 376
[81] Gevorkyan S R *et al* 1998 *Preprint* hep-ph/9804264
[82] Hofmann C, Soff G, Schäfer A and Greiner W 1991 *Phys. Lett.* B **262** 210
[83] Baron N and Baur G 1993 *Phys. Rev.* C **48** 1999
[84] Greiner M *et al* 1995 *Phys. Rev.* C **51** 911
[85] Weinberg S 1997 *The Quantum Theory of Fields* vol 1 (Cambridge: Cambridge University Press)
[86] Kolanoski H and Zerwas P 1988 *High Energy Electron–Positron Physics* ed A Ali and P Söding (Singapore: World Scientific)
[87] Berger Ch and Wagner W 1987 *Phys. Rep.* C **176** 1
[88] G Cochard and P Kessler (ed) $\gamma\gamma$ *Collisions, Proc., (Amiens 1980)* (*Lect. Notes Phys.* **134**) (Berlin: Springer)
[89] 1992 *Proc. 9th Int. Workshop on Photon–Photon Collisions (San Diego)* (Singapore: World Scientific)
[90] D J Miller *et al* (ed) 1995 *Photon'95, Xth Int.l Workshop on Gamma–Gamma Collisions and Related Processes* (Singapore: World Scientific)
[91] A Buijs (ed) 1997 *Photon'97, XIth Int. Workshop on Gamma–Gamma Collisions and Related Processes (Egmond aan Zee)* (Singapore: World Scientific)
[92] L3 collaboration 1997 *Phys. Lett.* B **408** 450
[93] Yang C N 1948 *Phys. Rev.* **77** 242
[94] Cooper S 1988 *Ann. Rev. Nucl. Part. Sci.* **28** 705
[95] Cartwright S *et al* 1998 *J. Phys. G: Nucl. Part. Phys.* **24** 457
[96] Godang R *et al* 1997 *Phys. Rev. Lett.* **79** 3829
[97] Telnov V 1995 *Photon '95, Sheffield* ed D J Miller *et al* (Singapore: World Scientific) p 369
[98] Ginzburg I F 1995 *Photon '95, Sheffield* ed D J Miller *et al* (Singapore: World Scientific) p 399
[99] Drees M, Ellis H and Zeppenfeld D 1989 *Phys. Lett.* B **223** 454
[100] Müller B and Schramm A J 1990 *Phys. Rev.* D **42** 3699
[101] Papageorgiu E 1995 *Phys. Lett.* B **352** 394
[102] Norbury J 1990 *Phys. Rev.* D **42** 3696
[103] Choudhury D and Krawczyk M 1997 *Phys. Rev.* D **55** 2774

[104] Renard F M 1983 *Phys. Lett.* B **126** 59
[105] Baur U, Fritzsch H and Faissner H 1984 *Phys. Lett.* B **135** 313
[106] 1996 *Future Physics at HERA* ed G Ingelman *et al* (Hamburg: DESY)
[107] Müller A H 1998 *Eur. Phys. J.* A **1** 19
[108] Engel R *et al* 1997 *Z. Phys.* C **74** 687
[109] Engel R private communication
[110] Müller B and Schramm A J 1991 *Nucl. Phys.* A **523** 677
[111] Schramm A J and Reeves D H 1997 *Phys. Rev.* D **55** 7312
[112] Nystrand J and Klein S 1997 Two photons physics at RHIC: separating signals from backgrounds *Hadron '97 (Brookhaven National Laboratory)* STAR Note 315, LBNL-41111
[113] Griffin J J 1998 The APEX/EPOS quandary: the way out via low energy studies *Proc. 8th Int. Conf. on Nuclear Reaction Mechanisms (Varenna, Italy, June 9–14 1997)* ed E Gadioli p 493 *Preprint* nucl-th/9802044
[114] Eichler J and Meyerhof W E 1995 *Relativistic Atomic Collisions* (San Diego, CA: Academic)
[115] Baur G 1990 *Phys. Rev.* A **42** 5736
[116] Heitler W 1954 *The Quantum Theory of Radiation* (London: Oxford University Press)
[117] Baur G 1990 *Phys. Rev.* D **41** 3535
[118] Best C, Greiner W and Soff G 1992 *Phys. Rev.* A **46** 261
[119] Rhoades-Brown M J and Weneser J 1991 *Phys. Rev.* A **44** 330
[120] Hencken K, Trautmann D and Baur G 1995 *Phys. Rev.* A **51** 998
[121] Hencken K, Trautmann D and Baur G 1995 *Phys. Rev.* A **51** 1874
[122] Güçlü M C *et al* 1995 *Phys. Rev.* A **51** 1836
[123] Bottcher C and Strayer M R 1989 *Phys. Rev.* D **39** 1330
[124] Alscher A, Hencken K, Trautmann D and Baur G 1997 *Phys. Rev.* A **55** 396
[125] Baron N and Baur G 1992 *Phys. Rev.* D **46** R3695
[126] Baur G and Baron N 1993 *Z. Phys.* C **60** 95
[127] Baur G 1992 *Nucl. Phys.* A **538** 187c
[128] Baron N and Baur G 1992 *Phys. Rev.* D **46** 4897
[129] Stekas J *et al* 1981 *Phys. Rev. Lett.* **47** 1686
[130] Bottcher C, Strayer M R, Albert C J and Ernst D J 1990 *Phys. Lett.* B **237** 175
[131] Landau L D and Lifschitz E M 1986 Quantenelektrodynamik *Lehrbuch der theoretischen Physik* vol 4 (Berlin: Akademie)
[132] Ivanov D and Melnikov K 1998 *Phys. Rev.* D **57** 4025
[133] Segev B and Wells J C 1998 *Phys. Rev.* A **57** 1849
[134] Eichmann U, Reinhardt J, Schramm S and Greiner W 1998 *Preprint* nucl-th/9804064
[135] Baltz A J and McLerran L 1998 *Phys. Rev.* C **58** 3
[136] Jackiw R, Kabat D and Ortiz M 1992 *Phys. Lett.* B **277** 148
[137] Baur G 1991 *Nucl. Phys.* A **531** 685
[138] Baltz A J, Rhoades-Brown M J and Weneser J 1992 *Phys. Rev.* A **44** 5569
[139] Baltz A J, Rhoades-Brown M J and Weneser J 1993 *Phys. Rev.* A **48** 2002
[140] Becker U, Grün N and Scheid W 1987 *J. Phys. B: At. Mol. Phys.* **20** 6563
[141] Aste A, Hencken K, Trautmann D and Baur G 1994 *Phys. Rev.* A **50** 3980
[142] Agger C K and Sørensen A H 1997 *Phys. Rev.* A **55** 402
[143] Rhoades-Brown M J, Bottcher C and Strayer M R 1989 *Phys. Rev.* A **40** 2831
[144] Meier H *et al* 1998 *Eur. Phys. J.* C in press
[145] Bertulani C A and Baur G 1998 *Phys. Rev.* D **58** 3
[146] Baltz A 1997 *Phys. Rev. Lett.* **78** 1231
[147] Krause H F *et al* 1998 *Phys. Rev. Lett.* **80** 1190
[148] Belkacem A *et al* 1993 *Phys. Rev. Lett.* **71** 1514
[149] Belkacem A *et al* 1994 *Phys. Rev. Lett.* **73** 2432
[150] Baur G *et al* 1996 *Phys. Lett.* B **368** 251
[151] Blanford G *et al* 1998 *Phys. Rev. Lett.* **80** 3037
[152] Munger C T, Brodsky S J and Schmidt I 1993 *Hyperf. Inter.* **76** 175
[153] Munger C T, Brodsky S J and Schmidt I 1994 *Phys. Rev.* D **49** 3228
[154] Baur G 1990 *Perspectives on Photon Interactions with Hadrons and Nuclei (Lect. Notes Phys.)* ed M Schumacher and G Tamas (Berlin: Springer) p 111